THE GEOLOGICAL SOCIETY OF AMERICA®

Reconciling along-strike disparity in slip displacement of the San Andreas fault, central California, USA

Jared T. Gooley[1,†], Glenn R. Sharman[2], and Stephan A. Graham[1]
[1]*Department of Geosciences, Stanford University, 450 Jane Stanford Way, Building 320, Stanford, California 94305, USA*
[2]*Department of Geosciences, University of Arkansas, Fayetteville, Arkansas 72701, USA*

ABSTRACT

The correlation of the ca. 23 Ma Pinnacles and Neenach volcanic complexes provides the most robust estimate on the timing and magnitude of Neogene right-lateral displacement on the San Andreas strike-slip fault system (California, United States). Displacement of ~315 km has been applied rigorously along the plate margin to guide reconstruction of offset paleogeographic features. We present new detrital zircon U-Pb geochronology from the La Honda and western San Joaquin basins to document sediment provenance and reevaluate compositional constraints on a hypothesized key cross-fault tie (i.e., Castle Rock–Recruit Pass submarine fan system). Whereas the Upper Oligocene–Lower Miocene Vaqueros Formation of the La Honda basin was likely recycled from or shared a similar southern Sierra Nevada–western Mojave source with the underlying Eocene stratigraphy, we found that the Temblor Formation of the central Temblor Range (e.g., Recruit Pass submarine fan) was derived directly from Late Cretaceous northern Salinian basement. Furthermore, the Carneros Sandstone of the northern Temblor Range had a central Sierra Nevada batholith source that was likely recycled during early Miocene unroofing of the underlying stratigraphy. Conversely, strata of the southwest San Joaquin basin have provenance characteristics that match more closely with those of the La Honda basin.

Our data preclude a contiguous Castle Rock–Recruit Pass submarine fan system across the San Andreas fault. These relationships are resolved by restoring the ca. 105–100 Ma basement of the northernmost Salinian block an additional ~45 km or greater farther south relative to the Sierra Nevada batholith during late Oligocene–early Miocene time. Inconsistency in displacement along the San Andreas fault with the coeval correlation of the Pinnacles–Neenach volcanic complex is reconciled by postdepositional Miocene–Quaternary off-fault NW-SE structural shortening via major thrusts and/or transrotation of the Tehachapi block, in combination with extension of the northern Salinian block. This additional displacement reduces the need for pre–28 Ma slip on the San Andreas or predecessor faults to resolve Cretaceous through Eocene cross-fault relationships and reconciles an early Miocene discrepancy with Pacific–North America relative plate motion. This study highlights the fact that displacement histories of major strike-slip faults are divergent across changing structural domains, and recognition of slip disparities can constrain the magnitude of deformation.

INTRODUCTION

The San Andreas fault system is one of the best-studied transform margins in the world and has had a profound impact on current understanding of the kinematic relationship between transform margins and the greater framework of plate tectonics (e.g., Atwater, 1970; Atwater and Molnar, 1973). The kinematic history of the San Andreas fault and other strike-slip fault systems globally has been largely constrained on the basis of displaced paleogeologic features, or piercing points, across the fault trace (e.g., Dickinson et al., 1972; Matthews, 1976; Graham, 1978). Age versus offset relationships between piercing points can be used to reconstruct the time-displacement history of strike-slip faulting, constraining the timing of fault initiation and slip rates. However, this simple concept can be complicated by a number of factors, including discrepancies between piercing points, strain partitioning, and off-fault strain. For example, discrepancies in strain markers have been attributed to complex off-fault deformation along the southern segment of the San Andreas fault (Powell, 1993; Darin and Dorsey, 2013), the Northern Anatolian fault zone (Armijo et al., 1999; Şengör et al., 2005), and other analogous plate boundary–scale strike-slip fault systems. Significant crustal shortening across the northern boundary of the Tibetan Plateau via thrusts was accommodated by slip along the Altyn-Tagh transform fault (Ritts et al., 2004; Zhang et al., 2014), and basement strain markers along the Alpine fault have been used to constrain the timing of intracontinental deformation of Zealandia (King, 2000; Mortimer, 2014, 2018; Lamb et al., 2016). In the case of the San Andreas fault system, such complexities may account for discrepancies in slip offsets that have long been noted between Pacific and North American relative plate motion (Dickinson and Wernicke, 1997).

This study revisited the central San Andreas fault system to demonstrate how incorporation of off-fault strain may better resolve time-displacement reconstructions, thus providing a case study that may be applied to other strike-slip fault systems. The ca. 28 Ma initiation of the modern San Andreas fault system (Atwater, 1989), and subsequent northward migration of the Mendocino triple junction and displacement of the Salinian block (Fig. 1), had significant consequential effects on the regional tectonic events of western North America. In central California, these included the demise of the Ancestral Cascade magmatic arc as the southern terminus of partial melting associated with the subducted Juan de Fuca plate migrated northward (Graham et al., 1984); reconfiguration of the Mesozoic Great Valley forearc basin and associated subduction complex along the central California margin into the Sacramento, San Joaquin, and adjacent basins of the Salinian block (Graham, 1978; Page, 1981; Bartow, 1991); and abrupt reorganizations in continental-scale paleodrainage to the California margin (Gooley et al., 2020).

Basement lithologies, volcanic centers, and paleogeographic features that formed across the San Andreas fault have subsequently been

Jared Thomas Gooley http://orcid.org/0000-0001-5620-3702
[†]gooleyjt@gmail.com.

GSA Bulletin; https://doi.org/10.1130/B35681.1; 15 figures; 3 tables; 1 supplemental file.

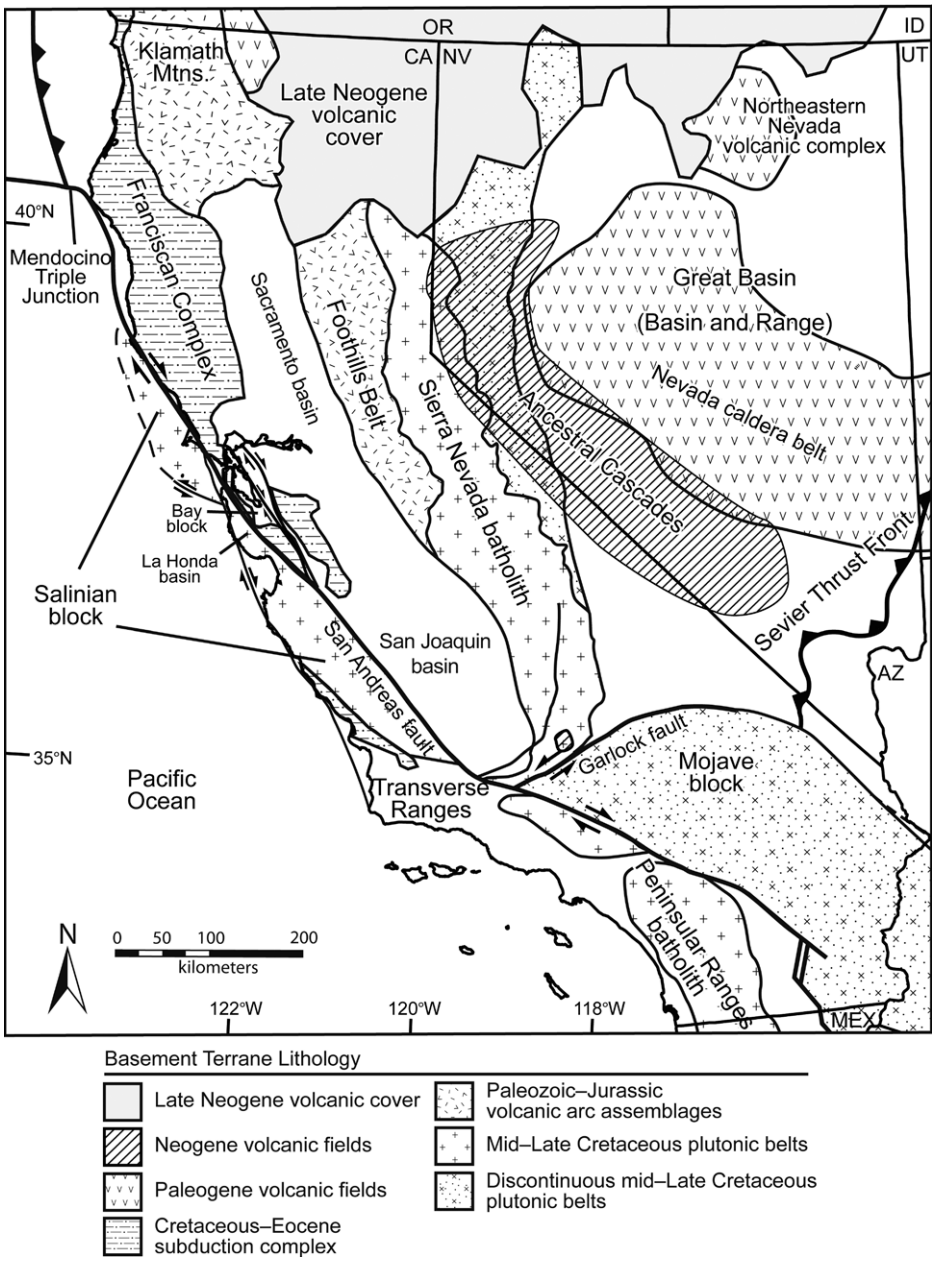

Figure 1. Regional geologic map of western United States showing main tectonic features and basement units discussed in the text. Map is modified from Dickinson (2008), Surpless and Beverly (2013), Sharman et al. (2015), Dumitru et al. (2015), and Gooley et al. (2020). State abbreviations: AZ—Arizona; CA—California; ID—Idaho; NV—Nevada; OR—Oregon; UT—Utah; MEX—Mexico.

displaced and provide constraints on the magnitude and timing of right-lateral slip (e.g., Huffman, 1972; Dickinson et al., 1972; Graham et al., 1989). Perhaps the most authoritative constraints on the long-term displacement history of the Salinian block are: (1) the ~415 km of right-lateral offset of the Cretaceous plutonic rocks at its inferred northern edge from the southern extent of the Cretaceous Sierra Nevada batholith (Figs. 1 and 2; Dickinson et al., 2005); and (2) the correlation of the ca. 23 Ma Pinnacles and Neenach volcanic complexes based on similar stratigraphy, geochemistry, and geochronologic constraints (Matthews, 1973, 1976). The estimated amount of 315 km of right-lateral slip since the eruption of the Pinnacles-Neenach volcanic center has been uniformly applied along the central and northern traces of the San Andreas fault to look for corroborating lithologic and paleogeographic features that were coeval with its initiation and early offset. These include inferred displacement of: (1) 280–305 km based on early Miocene shoreline and volcanic rocks (Dickinson et al., 1972); (2) 320–330 km based on late Oligocene and early Miocene paleobathymetric features in the La Honda and San Joaquin basins (Stanley, 1987); and (3) 320–330 km based on a petrographically and stratigraphically similar deep-water fan system that was interpreted to be contiguous across these basins (Graham et al., 1989).

Eocene geologic features were found to generally match these displacements, including the contiguous Eocene Butano–Point of Rocks deep-water fan system of the La Honda and San Joaquin basins that was reportedly displaced by 300–330 km (Clarke and Nilsen, 1973; Graham et al., 1989) and Eocene forearc strata and volcanics that were offset by an estimated 305–320 km (Nilsen, 1984). These constraints suggested that little to no displacement occurred on the modern San Andreas fault prior to 23 Ma. The remaining 100 km discrepancy in offset between the Cretaceous basement and Oligocene–Miocene Pinnacles-Neenach volcanic complexes led some workers to infer an earlier stage of right-lateral slip on the San Andreas fault or a predecessor fault ("two-stage slip" model; Fig. 3) during Late Cretaceous and/or Paleogene time (Suppe, 1970; Graham, 1978; Dickinson et al., 2005).

However, the cross-fault correlation of the Eocene Butano and Point of Rocks submarine fan (Clarke and Nilsen, 1973) was challenged on the basis of incompatible sandstone compositions, paleocurrent directions, and conglomerate clast lithologies (Seiders and Cox, 1992). Furthermore, using detrital zircon U-Pb geochronology, Sharman et al. (2013) confirmed that the Eocene Butano and Point of Rocks submarine fans did not share a similar provenance; therefore, the deep-water submarine fan system was not contiguous across the plate boundary and could not be used as a reliable piercing line for estimating fault displacement. Rather, the western Mojave and southern Sierran source of the Butano Sandstone suggests that the Salinian block was located an additional 50–75 km to the south relative to the Sierra Nevada batholith during Eocene time (Sharman et al., 2013). The most important implication of this finding was that Paleogene displacement (pre–Pinnacles-Neenach volcanic complexes) was required on the modern San Andreas fault. The additional ~100 km of displacement of Salinian plutonic rocks could have occurred either entirely on the early San Andreas fault system or as a combination with proto–San Andreas fault movement (Sharman et al., 2013; see revised models of Fig. 3).

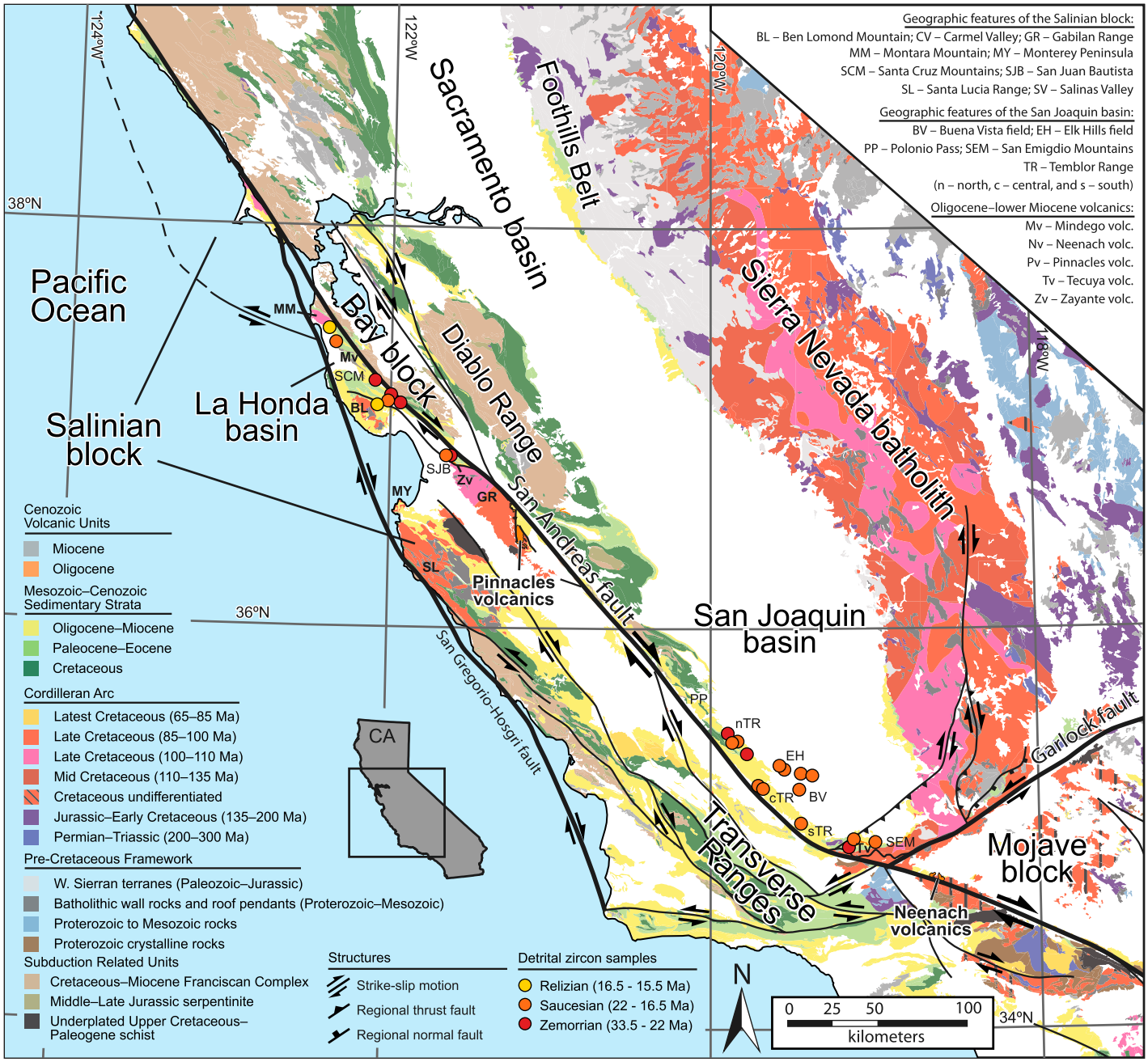

Figure 2. Geologic map of central California showing key faults, basement and volcanic units discussed in the text, and locations of detrital zircon samples in the San Joaquin basin and northern Salinian block presented in this study. Map location is shown on the inset of California (CA). Samples are colored by late Oligocene–middle Miocene benthic foraminiferal stages of western North America (refer to Fig. 4). Geologic units were modified from Jennings et al. (1997), Chapman et al. (2010), and Sharman et al. (2015).

In this study, we revisited the Oligocene–Lower Miocene deep-water fan systems and associated rocks of the northern Salinian block and western San Joaquin basin. In principle, if a sedimentary fan with a common sediment source had been deposited across the developing plate boundary and was subsequently offset, then the provenance of the strata within each half of the displaced unit would be indistinguishable. Specifically, we used detrital zircon U-Pb geochronology to evaluate the provenance of the Recruit Pass (Temblor Formation) and Castle Rock (Vaqueros Formation) deep-water fans and adjacent stratigraphy and test if these correlative systems were contiguous across the northern San Andreas fault (Graham et al., 1989). Our data challenge the Castle Rock–Recruit Pass fan correlation, and we propose a revised cross-fault correlation for the northern Salinian block and western San Joaquin basin. This correlation results in a greater slip displacement than previously recognized along the northern segment of the San Andreas fault, and we propose kinematic solutions for resolving apparent discrepancy in the magnitude of slip relative to the coeval Pinnacles-Neenach volcanic center.

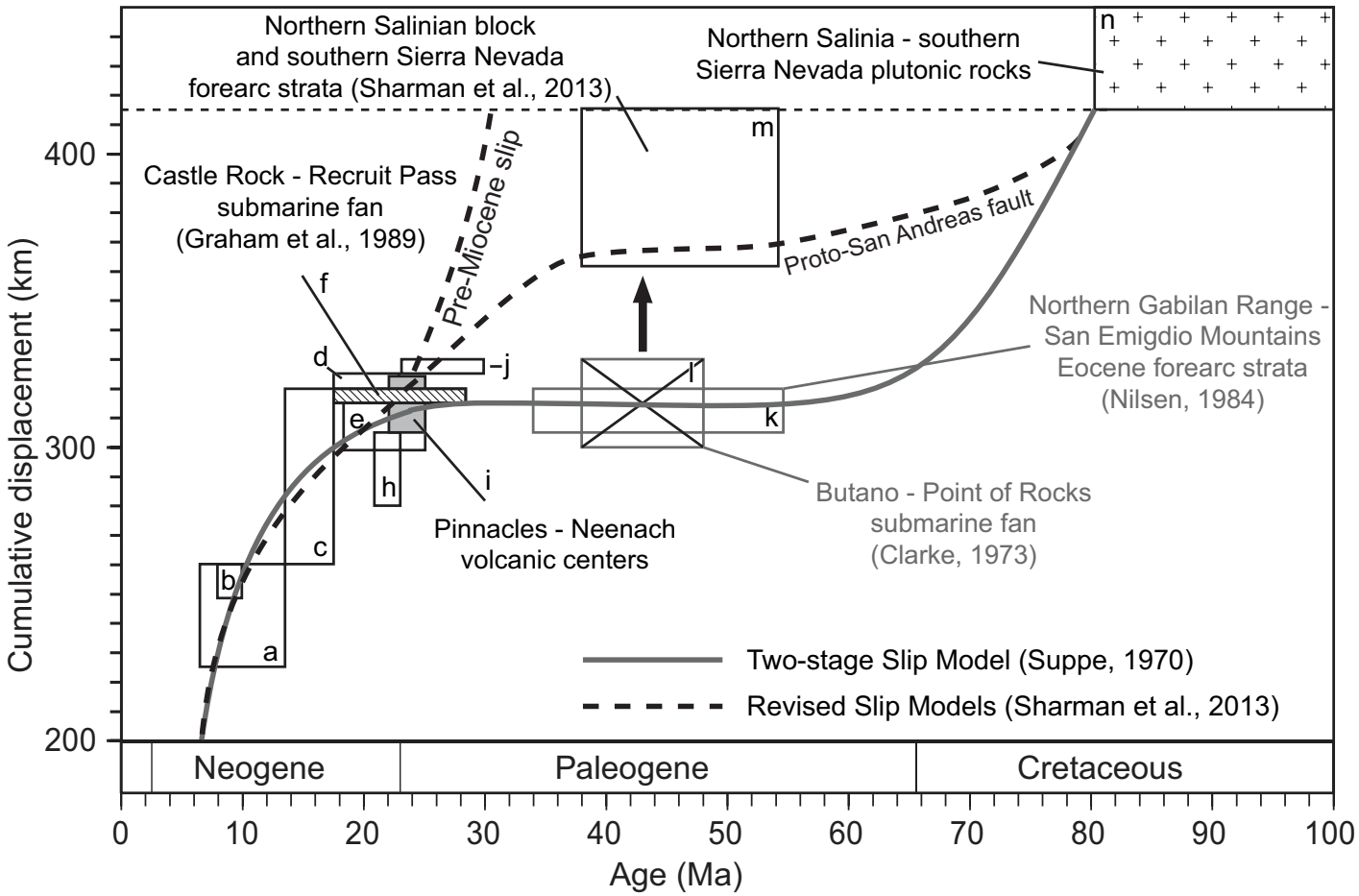

Figure 3. Alternative displacement histories of the San Andreas fault (boxes labeled with lowercase letters; see Table S2 [text footnote 1]). Correlations of the ca. 23 Ma Pinnacles and Neenach volcanic complexes and granitic rocks of the Cordilleran magmatic arc are the primary constraints on dextral displacement of the Salinian block. Previous Paleogene constraints suggested no displacement along the modern San Andreas fault prior to 23 Ma and that Salinian basement was initially separated by a proto–San Andreas fault (two-stage slip model; e.g., Suppe, 1970). Recent revision of the sediment source for Eocene strata of the northern Salinian block (Sharman et al., 2013) required an additional ~50–75 km of Paleogene displacement on the modern San Andreas fault. In this model, slip could have occurred entirely on the San Andreas or additionally on a predecessor fault. The correlation of the Oligocene–Miocene strata of the La Honda basin and western San Joaquin basin (hatchured box) that corroborate coeval Pinnacles-Neenach displacement was reevaluated in this study.

STUDY AREA AND STRATIGRAPHIC FRAMEWORK

Northern Salinian Block

The La Honda basin, which is bounded by the Cretaceous Salinian granitic rocks of Montara Mountain (ca. 104–102 Ma) to the north and Ben Lomond Mountain (ca. 99–92 Ma) to the south (Mattinson, 1994; Kistler and Champion, 2001), is currently expressed as the structurally complex and extensively vegetated outcrops of the Santa Cruz Mountains (Fig. 2). The western part of the basin has been displaced northward along the San Gregorio–Hosgri fault (Fig. 1; Dickinson et al., 2005). The La Honda basin has a composite stratigraphic thickness of more than 14 km of sedimentary and volcanic strata (Stanley, 1990). Subsidence of the early La Honda basin is thought to have initiated during the Paleocene, possibly associated with transpressional tectonics due to oblique subduction, and this was enhanced during Oligocene–Miocene time as a result of transtension along the newly developing San Andreas fault (Stanley, 1990).

The Eocene deep-water Butano Sandstone, deposited during the early phase of basin formation, is exposed along the northern and southern flanks of the La Honda basin. Stanley (1985) described the Oligocene and Miocene strata of the La Honda basin in detail, as summarized in Figure 4A. This study focused on the sandstone facies of the Upper Oligocene through Lower Miocene Vaqueros Formation and equivalent stratigraphy. Two thick, stratigraphically distinct units of deep-water sandstone are recognized on the northern and southern margins of the basin.

Figure 4. Stratigraphic correlation and lithostratigraphy of (A) the northern Salinian block and (B) western San Joaquin basin. Note time scale change after 20 Ma. Relative stratigraphic positions of detrital zircon samples are indicated (see Table 1 for details). Sampled sandstone units are color coordinated with Figures 5, 6, 7, 9, 10, and 11. L—late; M—middle; E—early; Sst—Sandstone; Sh—Shale; Fm—Formation; Mbr—Member.

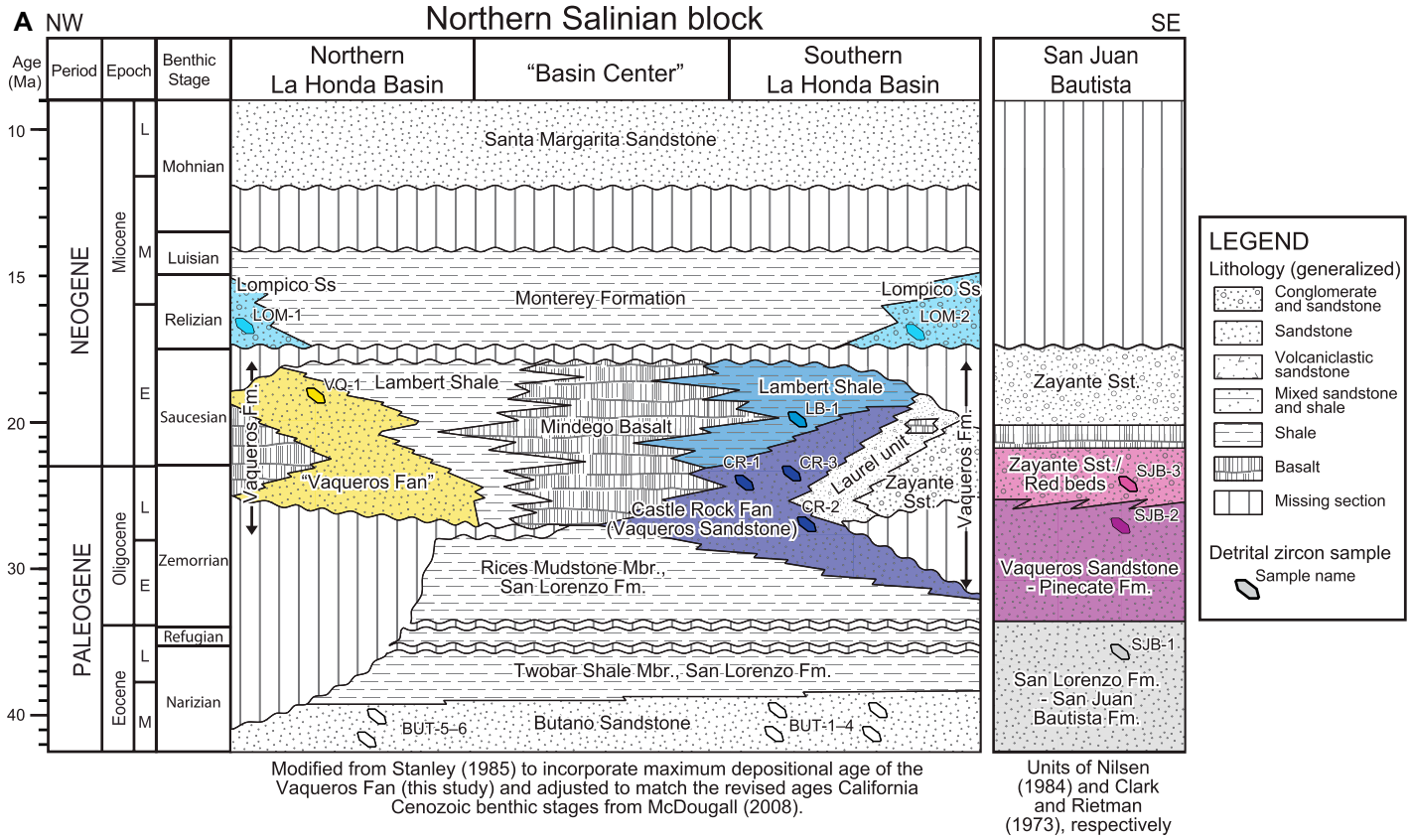

Modified from Stanley (1985) to incorporate maximum depositional age of the Vaqueros Fan (this study) and adjusted to match the revised ages California Cenozoic benthic stages from McDougall (2008).

Units of Nilsen (1984) and Clark and Rietman (1973), respectively

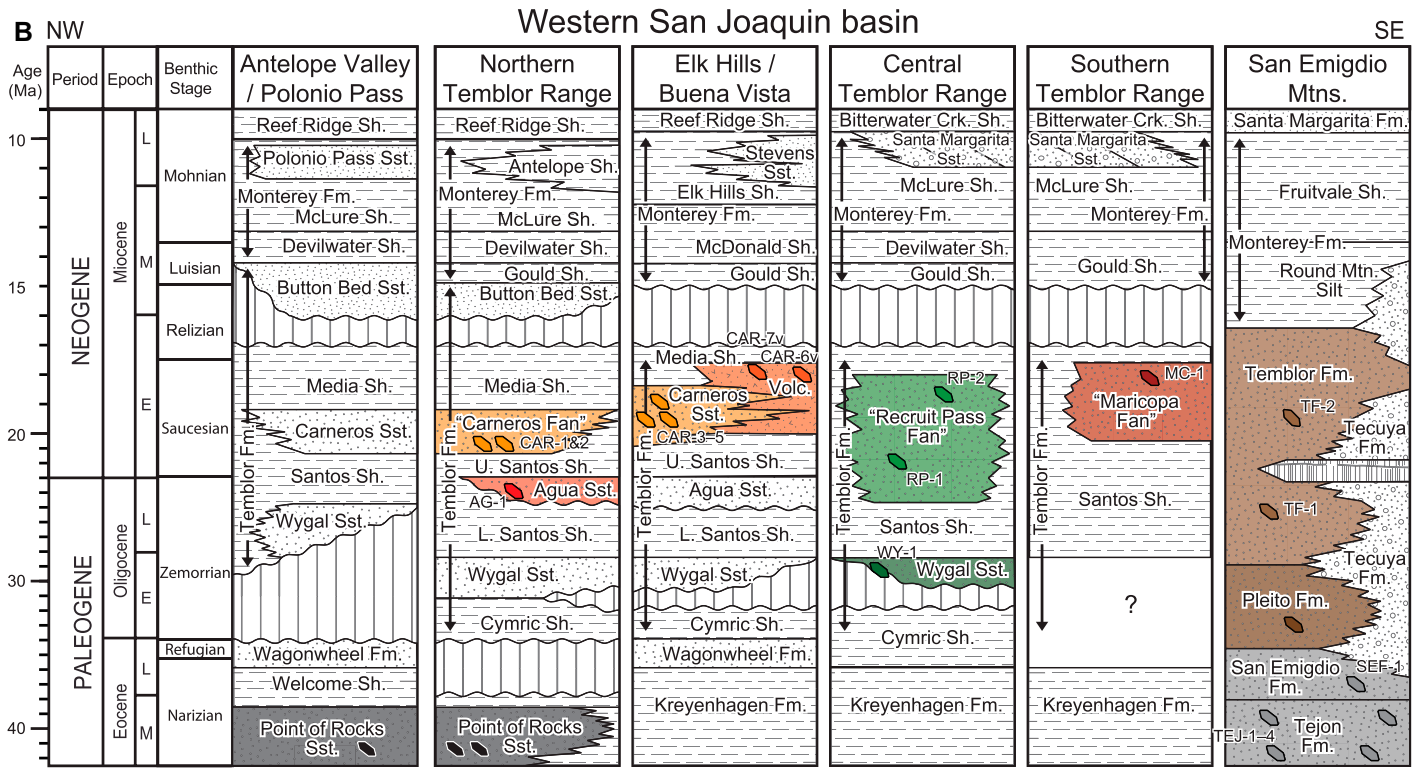

Modified from Johnson and Graham (2007)

Modified from Johnson and Graham (2007)

Modified from Graham et al. (1989); Bartow (1991); Reid (1995).

Units from Dibblee (1973); Graham et al. (1989); Ryder and Thomson (1989)

Units from Dibblee (1973); Graham et al. (1989); Ryder and Thomson (1989)

Modified from Bartow (1991); Reid (1995).

The northern Vaqueros submarine fan is poorly exposed, but it generally thins southwards (Stanley, 1985) and contains granitic detritus and radiolarian chert grains that were interpreted to have been derived from the northern Salinian basement and Franciscan subduction complex, respectively (Graham et al., 1989). The southern Castle Rock submarine fan was derived from a granitic source, has generally northward- and eastward-trending paleocurrents, and is the distal deep-water equivalent to the shallow-marine shelf sandstone of the Laurel Unit and coarse-grained fan delta facies of the Zayante Sandstone (Fig. 4A). At the center of the basin, the sandstone and distal shale units interstratify with over 1500 m of volcanics (e.g., the Mindego Basalt; Fig. 4A). Stanley (1985) interpreted the Mindego Basalt to have been erupted by a submarine volcanic complex in the center of a pull-apart basin, with laterally adjacent siliciclastic units shed off the flanks of the granitic basement highs filling the rapidly subsiding basin.

The Middle Miocene siliceous and calcareous mudstone of the Monterey Formation unconformably overlies the Lower Miocene units and is generally laterally correlative to the north and south with the shallow-marine Lompico Sandstone (Fig. 4A), the northern exposure of which directly onlaps the granitic basement of Montara Mountain. The next closest southward exposure of Eocene through Lower Miocene stratigraphy (Fig. 4A) is greater than 30 km to the south, just west of the current trace of the San Andreas fault near San Juan Bautista (Fig. 2).

Western San Joaquin Basin

The Neogene San Joaquin basin is the southern remnant of the Cretaceous–early Neogene Great Valley forearc basin (Fig. 1) that was overprinted by strike-slip tectonism of the San Andreas fault system, including translation of the Salinian block in late Cenozoic time. The basin is bounded on the east and southeast by the southern half of the Cretaceous Sierra Nevada batholith. To the northwest, the southern extent of the Diablo Range (Fig. 2) is composed primarily of Cretaceous Franciscan subduction complex that has been uplifted by pre– and syn–San Andreas fault–related transpression (Wentworth et al., 1984; Bloch et al., 1993). The Temblor Range consists of exhumed Cenozoic basin fill along the trace of the San Andreas fault. To the south, the strata of the San Emigdio Mountains have been exhumed by series of northward-verging thrusts north of the Garlock fault (Fig. 2).

The Eocene through Upper Miocene stratigraphy of the western San Joaquin basin is summarized in Figure 4B. The Eocene Point of Rocks Sandstone of the deep-water Kreyenhagen Formation is only exposed in outcrop as far south as the northern Temblor Range, but the unit persists southwestward into the subsurface. Previously thought to have been sourced by granitic highlands from the southwest side of the San Andreas fault (e.g., Clarke and Nilsen, 1973), northwest-directed paleoflow indicators (Nilsen and Simoni, 1973) and detrital zircon geochronologic data suggest that the deep-water Point of Rocks Sandstone was derived from the Sierra Nevada batholith to the east (Sharman et al., 2013).

During Oligocene time, evolving tectonic conditions associated with the early development of the transform plate margin caused rapidly changing basin conditions in the western margin of the San Joaquin basin that are recorded in the strata of the Temblor Formation (Carter, 1985). In particular, lower members of the Temblor Formation record episodes of uplift (e.g., shallow marine Wygal Sandstone) and deepening (e.g., Santos Shale) that culminated in the deposition of three distinct submarine fan systems during the late Zemorrian (late Oligocene) through Saucesian (early Miocene) benthic stages (Fig. 4B; Graham et al., 1989). These deep-water sandstone units were deposited in middle and lower bathyal paleowater depths (Simonson and Krueger, 1942; Graham et al., 1989), and paleobathymetric maps based on benthic foraminiferal paleoecology portray the Zemorrian and Saucesian stages of the San Joaquin basin to have had a bathymetric low south of Bakersfield and place the Temblor Range on the western upslope side of the northeastward-deepening basin (Bandy and Arnal, 1969).

The northernmost "Carneros submarine fan" (Fig. 4B) consists of the Carneros Sandstone Member of the Temblor Formation, where exposed in the northern Temblor Range, and projects southwestward into the subsurface (Pence, 1985), where it is penetrated by wells at Elk Hills and Buena Vista fields. Carneros submarine fan sandstone contains detrital radiolarian chert and porphyritic felsite that were likely sourced from the exposed Mesozoic Franciscan subduction complex and Cretaceous Great Valley Group of the southern Diablo Range (Fig. 2; Pence, 1985; Graham et al., 1989). Southeast of the Carneros fan in the San Joaquin basin subsurface, a volcanic-rich sandstone unit of unknown origin is present (Gordon et al., 2017), and the stratigraphic relationship has not been fully determined ("Volc." unit of Elk Hills/Buena Vista fields; Fig. 4B). However, similar ash-rich units have been reported within the underlying Upper Santos Shale (Reid, 1995), and these deposits may be equivalent or derived from a similar source. The "Recruit Pass submarine fan" is exposed in the central Temblor Range and is separated from the Carneros fan by a northwest-southeast–trending submarine paleotopographic high (the Belgian anticline). In contrast to the Carneros fan, Recruit Pass submarine fan sandstone is dominated by granitic detritus and additionally contains basalt fragments instead of radiolarian chert and porphyritic felsite fragments (Bent, 1985; Graham et al., 1989). Finally, the "Maricopa submarine fan" is exposed in the southernmost Temblor Range and San Emigdio Mountains (Fig. 4B; Graham et al., 1989). Bent (1985) described the Temblor Formation sandstone of the Maricopa fan as compositionally enriched in basalt grains and recycled sedimentary lithics, and Gillespie (1986) presented evidence of a northward-directed paleocurrent. These authors interpreted the sediment to have been locally derived from Paleocene sandstones juxtaposed across the San Andreas fault.

An unconformity related to late Saucesian uplift separates the Relizian transgressive, shallow-marine, bioclastic Button Bed Sandstone from the underlying deep-water units in the Temblor Formation (Carter, 1985). Although traditionally grouped with the Temblor Formation, this unit is genetically linked with the overlying biosiliceous bathyal mudstone of the Monterey Formation. Together, the Button Bed Sandstone and Monterey Formation record a rapid trend in subsidence in the basin (Graham et al., 1989).

La Honda–San Joaquin Correlation

While recognizing spatial and temporal uncertainties in the preferred realignment of the Pinnacles-Neenach volcanic centers (Matthews, 1973) and corroborating shoreline, volcanic, and paleobathymetric features of the southern San Joaquin basin (Dickinson et al., 1972; Stanley, 1987), Graham et al. (1989) considered the petrologic composition of the Oligocene and Lower Miocene strata (Fig. 5) and found that the juxtaposition of the La Honda and San Joaquin basins favorably aligned the Vaqueros and Temblor Formation sediment dispersal systems (Fig. 6). Although Graham et al. (1989) acknowledged that pre–middle Miocene tectonic rotation of the southern San Joaquin basin remained to be addressed (Kanter and McWilliams, 1982; McWilliams and Li, 1985; Plescia and Calderone, 1986), they found that northeastward-trending paleocurrent indicators, granitic sandstone petrofacies, and inferred subsurface geometry of the thick-bedded Castle Rock and Recruit Pass deep-water fan systems were similar and interpreted 315–320 km of right-lateral slip along the San Andreas fault. Similarly, based on this preferred alignment, Reid (1995) determined that volcanic vents associated with the Mindego Basalt of the La Honda basin were the likely source of ash and tuff deposits within the western San Joaquin basin (e.g., volcanic-rich Carneros Sandstone).

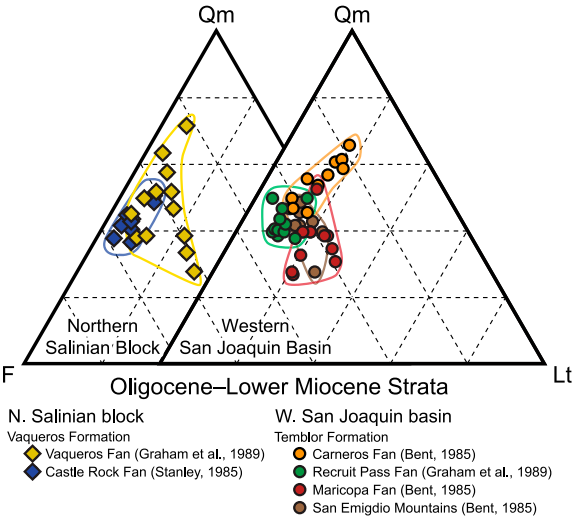

Figure 5. Published detrital compositional relationships in sandstones of the northern Salinian block (La Honda basin) and western San Joaquin basin. Ternary plot of sand grain fractions from Oligocene–Lower Miocene sandstone samples (after Bent, 1985; Stanley, 1985; Graham et al., 1989) is shown in terms of monocrystalline quartz (Qm), feldspar (F), and total rock fragments (Lt).

METHODS

Sampling Strategy

In total, 24 new samples from Upper Oligocene to Middle Miocene sandstones were analyzed in this study (2296 analyses). We collected nine outcrop samples throughout the Salinian block (Fig. 4A) and 10 outcrop and five subsurface (core) samples along the west side of the San Joaquin basin (Fig. 4B) in order to characterize provenance trends along a wide range of latitude on each side of the plate margin when ~315 km of slip is restored on the San Andreas fault (Fig. 6). We also included one previously published Upper Oligocene sample from the San Emigdio Mountains (Shulaker et al., 2019). Where

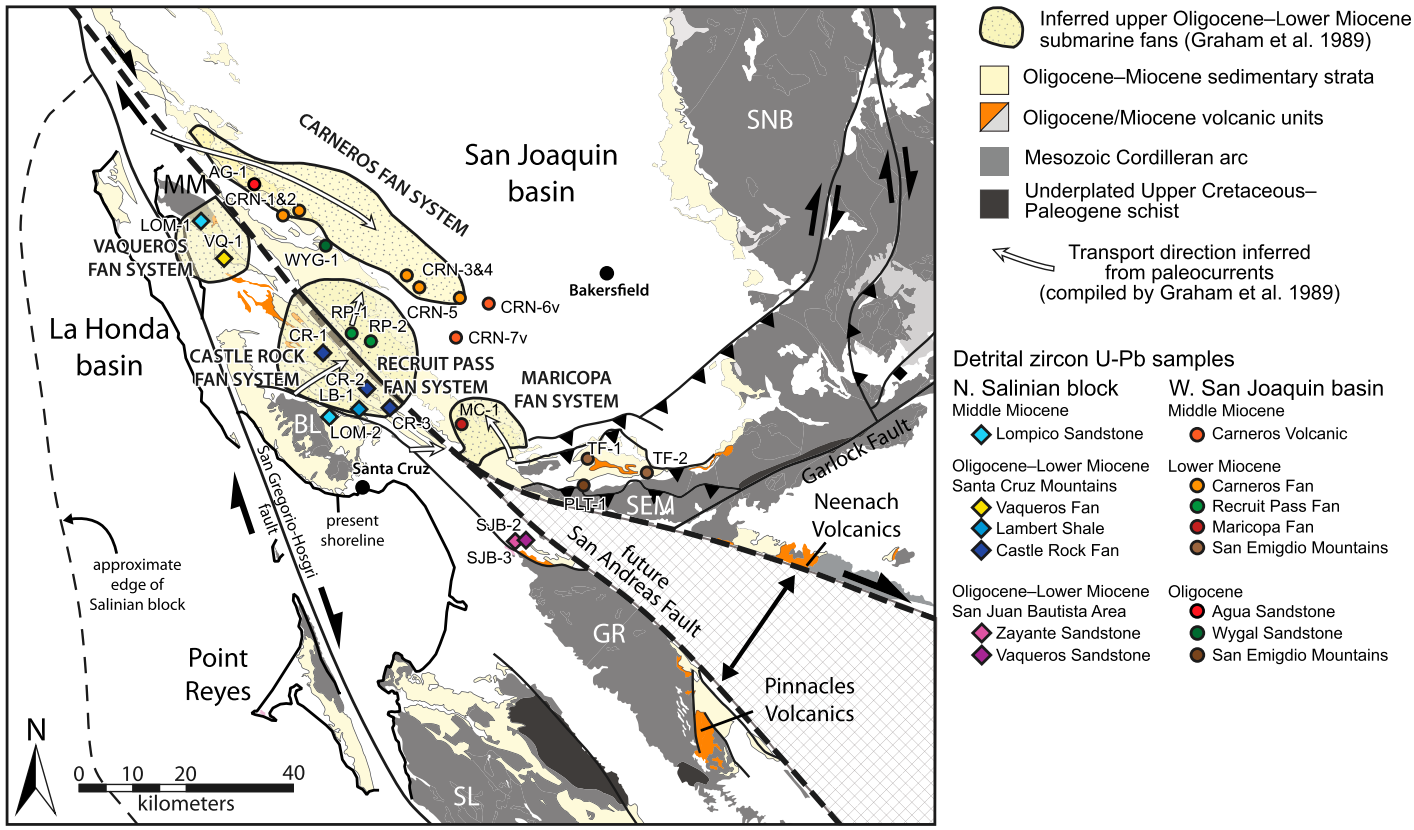

Figure 6. Paleogeographic reconstruction of central California during late Oligocene–early Miocene time as visualized prior to this study. Palinspastic restoration of ~315 km of slip on the San Andreas fault aligns the ca. 23 Ma Neenach and Pinnacles volcanic complexes (Matthews, 1973, 1976) and late Zemorrian through early Saucesian stage paleobathymetry of the La Honda and San Joaquin basins (Stanley, 1985). Slip on the Garlock fault is not restored, and treatment of the Salinian block as a rigid object during restoration produces a gap (cross-hatched area) due to the bend in the San Andreas fault. Additionally, ~155 km of late Miocene–Quaternary slip on the San Gregorio–Hosgri fault has been removed (Dickinson et al., 2005; Sharman et al., 2015). Interpreted sediment dispersal systems investigated in this study are shown, including the correlative Castle Rock and Recruit Pass deep-water submarine fans (Graham et al., 1989). Locations of sandstone samples for detrital zircon U-Pb geochronology are indicated. Geographic features: BL—Ben Lomond Mountain; GR—Gabilan Range; MM—Montara Mountain; SEM—San Emigdio Mountains; SL—Santa Lucia Range; SNB—Sierra Nevada batholith.

possible, samples were preferentially selected directly from or near localities previously analyzed for sandstone petrography (e.g., Bent, 1985; Stanley, 1985; Graham et al., 1989) and where biostratigraphic constraints on benthic foraminiferal stage (Zemorrian–Relizian) were well established (Fig. 2). Each sample consisted of fine- to coarse-grained sandstone and was analyzed for detrital zircon U-Pb geochronology.

Compilation of Published Detrital Zircon Data

We also compiled previously published detrital zircon U-Pb distributions measured from Middle Eocene sandstone units of the northern Salinian block and western San Joaquin basin. These units stratigraphically underlie those analyzed in this study and allow both temporal comparison of provenance trends and evaluation of local sediment recycling during the early development of the plate boundary. Sources for Eocene data included: (1) nine samples (810 total analyses) from the La Honda basin and San Juan Bautista area of the northern Salinian block (Sharman et al., 2013; Jacobson et al., 2011); and (2) eight samples (802 total analyses) from the western and southern San Joaquin basin (northern Temblor Range and San Emigdio Mountains; Lechler and Niemi, 2011; Sharman et al., 2013; Saleeby et al., 2016). Figure 4 shows the relative stratigraphic positions of sandstone samples in the northern Salinian block and western San Joaquin basin, and Table 1 provides the sample locations, ages, and stratigraphic units from which they were acquired.

Detrital Zircon U-Pb and Th/U Analytical Methods

About 2–5 kg rock samples were collected from each outcrop, and ~250–500 g samples were collected for each core sample. Detrital zircon grains were concentrated after crushing and disaggregating in Stanford's Earth Materials laboratory by applying standard hydrodynamic, magnetic, and density separation techniques (Appendix S1[1]). Measurement of detrital zircon U-Pb ages (100–200 analyses each) was performed at both the University of California–Santa Cruz (UCSC) and the University of Arizona LaserChron Center (ALC) following the standard laser-ablation–inductively coupled plasma–mass spectrometry (LA-ICP-MS) methods described by Gehrels et al. (2008). Data reduction methods for results obtained from UCSC have been described by Sharman et al. (2013). Additional details for analytical methods and the full data tables are presented in the data supplement (Appendix S1; Tables S3 and S4). The measured U-Pb ages were filtered using the following criteria: (1) $^{206}Pb/^{204}Pb > 200$, U-Pb discordance

[1]Supplemental Material. Appendix S1: Sample preparation and analytical methods; Table S1: Original sample names; Table S2: San Andreas fault offset estimates used in Figures 3 and 15; Tables S3 and S4: U-Th-Pb data; Table S5: Modern river and Eocene Th/U data sources; Table S6: Major structures with NW-SE deformation. Please visit https://doi.org/10.1130/GSAB.S.12947168 to access the supplemental material, and contact editing@geosociety.org with any questions.

TABLE 1. DETRITAL ZIRCON SAMPLE LOCATIONS

Sample	Formation	Unit	Age	Benthic stage	Area	Latitude (°N)	Longitude (°W)	Source
Middle–Upper Miocene								
LOM-1	Lompico Fm.		M. Miocene	Relizian	Santa Cruz Mtns. North	37.487716	122.395501	This study
LOM-2	Lompico Fm.		M. Miocene	Relizian	Santa Cruz Mtns. South	37.100320	122.034010	This study
Oligocene–Lower Miocene								
VQ-1	Vaqueros Fm.	Vaqueros Fan	E. Miocene	Sauc.	Santa Cruz Mtns. North	37.418290	122.351750	This study
LB-1	Lambert Shale	Castle Rock Fan	E. Miocene	Sauc.	Santa Cruz Mtns.	37.128580	122.017810	This study
CR-1	Vaqueros Fm.	Castle Rock Fan	L. Oligocene	Zem.	Santa Cruz Mtns. South	37.227500	122.096639	This study
CR-2	Vaqueros Fm.	Castle Rock Fan	L. Oligocene	Zem.	Santa Cruz Mtns. South	37.157528	122.001333	This study
CR-3	Vaqueros Fm.	Castle Rock Fan	L. Oligocene	Zem.	Santa Cruz Mtns. South	37.117861	121.943333	This study
SJB-2	Vaqueros Fm.	Vaqueros Sst.	L. Oligocene	Zem.	San Juan Bautista	36.863583	121.616100	This study
SJB-3	Vaqueros Fm.	Zayante Sst.	E. Miocene	Sauc.	San Juan Bautista	37.842525	121.944688	This study
AG-1	Temblor Fm.	Agua Sst.	Oligocene	Zem.	Temblor Range North	35.481157	119.895668	This study*
CRN-1	Temblor Fm.	Carneros Fan	E. Miocene	Sauc.	Temblor Range North	35.444760	119.857710	This study
CRN-2	Temblor Fm.	Carneros Fan	E. Miocene	Sauc.	Temblor Range North	35.443540	119.847340	This study
CRN-3	Temblor Fm.	Carneros Fan	E. Miocene	Sauc.	Elk Hills Field	35.315250	119.582076	This study
CRN-4	Temblor Fm.	Carneros Fan	E. Miocene	Sauc.	Elk Hills Field	35.303827	119.549115	This study
CRN-5	Temblor Fm.	Carneros Fan	E. Miocene	Sauc.	Elk Hills Field	35.281665	119.446324	This study
CRN-6v	Temblor Fm.	Carneros (Volc.)	E. Miocene	Sauc.	Elk Hills Field	35.273532	119.383613	This study
CRN-7v	Temblor Fm.	Carneros (Volc.)	E. Miocene	Sauc.	Buena Vista Field	35.198324	119.460764	This study
WYG-1	Temblor Fm.	Wygal Sst.	Oligocene	Zem.	Temblor Range North	35.377998	119.778618	This study*
RP-1	Temblor Fm.	Recruit Pass Fan	E. Miocene	Sauc.	Temblor Range Central	35.216500	119.710750	This study
RP-2	Temblor Fm.	Recruit Pass Fan	E. Miocene	Sauc.	Temblor Range Central	35.204315	119.680474	This study
MC-1	Temblor Fm.	Maricopa Fan	E. Miocene	Sauc.	Temblor Range South	35.027409	119.449065	This study
PLT-1	Pleito Fm.		Oligocene	Zem.–Sauc.	San Emigdio Mtns.	34.913917	119.160694	This study
TF-1	Temblor Fm.	Lower Temblor	L. Oligocene	Zem.–Sauc.	San Emigdio Mtns.	34.952056	119.131306	Shulaker et al. (2019)
TF-2	Temblor Fm.	Upper Temblor	E. Miocene	Sauc.	San Emigdio Mtns.	34.935313	118.998644	This study*
Paleocene–Eocene								
BUT-1	Butano Sst.		E.–M. Eocene	Ulat.–Nariz.	Santa Cruz Mtns. South	37.142667	122.190139	Sharman et al. (2013)
BUT-2	Butano Sst.		E.–M. Eocene	Ulat.–Nariz.	Santa Cruz Mtns. South	37.159300	122.235000	Sharman et al. (2013)
BUT-3	Butano Sst.		E.–M. Eocene	Ulat.–Nariz.	Santa Cruz Mtns. South	37.198889	122.196389	Sharman et al. (2013)
BUT-4	Butano Sst.		E.–M. Eocene	Ulat.–Nariz.	Santa Cruz Mtns. South	37.232306	122.232306	Sharman et al. (2013)
BUT-5	Butano Sst.		E.–M. Eocene	Ulat.–Nariz.	Santa Cruz Mtns. North	37.378500	122.263700	Sharman et al. (2013)
BUT-6	Butano Sst.		E.–M. Eocene	Ulat.–Nariz.	Santa Cruz Mtns. South	37.142699	122.188864	Jacobson et al. (2011)
SJB-1	San Juan Bautista Fm.		E.–M. Eocene	Ulat.–Nariz.	San Juan Bautista	36.862722	121.600694	Sharman et al. (2013)
POR-1	Point of Rocks Sst.		M. Eocene	Ulat.–Nariz.	Antelope Valley	35.727267	120.018117	Sharman et al. (2013)
POR-2	Point of Rocks Sst.		M. Eocene	Ulat.–Nariz.	Temblor Range North	35.437720	119.848090	Sharman et al. (2013)
POR-3	Point of Rocks Sst.		M. Eocene	Ulat.–Nariz.	Temblor Range North	35.381750	119.779139	Sharman et al. (2013)
TEJ-1	Tejon Fm.	Uvas Congl.	E.–M. Eocene	Ulat.–Nariz.	San Emigdio Mtns.	34.899472	119.150056	Sharman et al. (2013)
TEJ-2	Tejon Fm.	Metralla Sst.	M. Eocene	Ulat.–Nariz.	San Emigdio Mtns.	34.905972	119.156528	Sharman et al. (2013)
TEJ-3	Tejon Fm.	Uvas Congl.	E.–M. Eocene	Ulat.–Nariz.	San Emigdio Mtns.	34.943470	119.251540	Lechler and Niemi (2011)
TEJ-4	Tejon Fm.		E.–M. Eocene	Ulat.–Nariz.	San Emigdio Mtns.	34.896030	119.100410	Saleeby et al. (2016)
SEF-1	San Emigdio Fm.		L. Eocene	Nariz.	San Emigdio Mtns.	34.917056	119.168083	Sharman et al. (2013)

Note: Coordinates are in World Geodetic System 1984 (WGS84). Fm.—Formation; Sst.—Sandstone; Congl.—Conglomerate; Volc.—volcanics; Mtns—Mountains; E.—Early; M.—Middle; L.—Late; Nariz.—Narizian; Ulat.—Ulatisian; Zem.—Zemorrian; Sauc—Saucesian.
*Hand samples from Bent (1985); see Supplemental Material (text footnote 1) for original sample names.

<20%, and maximum reverse discordance <5%. U concentration and U/Th ratio were calibrated relative to the Sri Lanka zircon standard. Cumulative density plots (CDPs), kernel density estimate (KDE) plots, and plots of Th/U ratios were generated using detritalPy (Sharman et al., 2018).

Detrital Zircon Statistical Methods

Detrital Zircon Maximum Depositional Age Calculations

We used our detrital zircon U-Pb age results to calculate maximum depositional ages (MDAs) for our samples in an effort to further resolve ambiguous biostratigraphic and geochronologic constraints. The MDAs provided constraints for the correlation of time-equivalent stratigraphic units within the La Honda and San Joaquin basins. The presence of coeval volcanism in central California and surrounding regions (e.g., Stanley 1985, 1990) provides a reasonable expectation for finding young detrital zircon that is needed for MDA estimates to be useful in constraining depositional age (Sharman and Malkowski, 2020). Following Dickinson and Gehrels (2009) and Coutts et al. (2019), we present estimates based upon three different approaches (Table 2): (1) the youngest single grain age (YSG); (2) the weighted mean age of the youngest cluster of at least two ages within a 1σ error (YC1σ2+); and (3) the weighted mean age of the youngest cluster of at least three ages within a 2σ error (YC2σ3+). Grain clusters were defined following the approach outlined in Sharman et al. (2018). In 16 of 19 samples that yielded any Oligocene–Miocene zircon, the calculated YC1σ2+ age was within <3.0% error of the YC2σ3+ age. We used the YC1σ2+ age as our preferred MDA for these samples, as Dickinson and Gehrels (2009) demonstrated that the YC1σ2+ age underestimated a depositional age in only <5% of their samples. For two samples, only the YSG yielded a Cenozoic MDA, which, in both cases, was consistent with biostratigraphic constraints (Table 2). Coutts et al. (2019) suggested that the YSG age is preferable for samples with 50–100 analyses but warned that this method is susceptible to contamination or disturbance of the U-Pb systematics of zircon (e.g., lead loss), as illustrated by Herriott et al. (2019). We therefore placed greater confidence in MDA calculations based on multiple grain clusters versus the YSG.

Multidimensional Scaling

We used nonmetric multidimensional scaling (MDS) to assess the degree of dissimilarity between samples and further infer potential shared sediment source areas. Following the methods of Vermeesch (2013), detrital zircon age distributions were mapped together on a dimensionless plot to graphically display similarity. We used the Kolmogorov-Smirnov D_{max} (maximum separation between CDPs of sample pairs) as a similarity metric (Saylor and Sundell, 2016; Sharman et al., 2018). Samples that plot in proximity on the MDS plot are more similar (i.e., lower D_{max}) than samples that plot farther apart.

RESULTS

Detrital Zircon U-Pb Age Distributions

U-Pb age data were organized from north-to-south for the Salinian block and San Joaquin basin and are graphically displayed as KDEs in Figure 7. The proportions of key age fractions (sensu Andersen et al., 2018) that correspond to known basement ages (Figs. 1 and 2) are presented in Table 3, and fault-parallel trends in age fraction proportions are shown in Figure 7. The age fractions recognized in this study can be broadly grouped into three categories based upon geologic relationships throughout the western North American Cordillera: (1) pre-Permian zircon assemblages of the Laurentian provinces and Paleozoic terranes of the North American interior (older than ca. 300 Ma); (2) Permian–Paleogene Cordilleran arc assemblages (ca. 285–53 Ma); and (3) Paleogene–Neogene volcanic centers (ca. 52–10 Ma).

Northern Salinian Block

The Oligocene–Lower Miocene Vaqueros Formation of the La Honda basin (Santa Cruz Mountains) has a diverse assemblage of detrital zircon ages (Fig. 7). All samples were dominated by mid- to Late Cretaceous (135–85 Ma; 50%–71%) age fractions, although peak ages differed, with a subordinate fraction of Jurassic to Early Cretaceous (200–135 Ma), and minor fractions of Permian to Triassic (300–200 Ma), pre-Permian (>300 Ma), and Oligocene to Miocene

TABLE 2. SUMMARY OF DETRITAL ZIRCON MAXIMUM DEPOSITIONAL AGE (MDA) CALCULATIONS FOR OLIGOCENE–MIOCENE SAMPLES

Sample	Formation	Unit	Total grains	Youngest single grain (Ma ± 1σ)	Youngest overlapping cluster within 1σ error			Youngest overlapping cluster within 2σ error			Preferred MDA	Type
					YC1 (2+): (Ma ± 1σ)	MSWD	No. grains	YC2 (3+): Ma ± 1σ	MSWD	No. grains	(Ma ± 1σ)	
LOM-1	Lompico Fm.		107	92.6 ± 0.9	92.7 ± 0.9	0	2	93.8 ± 0.7	2	3	NA	NA
LOM-2	Lompico Fm.		116	82.1 ± 2.4	83.6 ± 1.1	0.5	2	89.7 ± 0.6	0.4	8	NA	NA
VQ-1	Vaqueros Fm.	Vaqueros fan	105	18.4 ± 0.8	18.6 ± 0.5	0.2	6	18.6 ± 0.4	0.2	6	18.6 ± 0.4	YC1(2+)
LB-1	Lambert Sh.	Castle Rock fan	99	23.8 ± 1.2	23.9 ± 1.0	0.1	2	24.9 ± 0.9	1.1	4	23.9 ± 1.0	YC1(2+)
CR-1	Vaqueros Fm.	Castle Rock fan	97	24.0 ± 1.1	24.0 ± 1.0	0.1	2	86.3 ± 0.6	2.7	4	24.0 ± 1.0	YC1(2+)
CR-2	Vaqueros Fm.	Castle Rock fan	101	26.7 ± 1.2	26.6 ± 1.1	0.1	2	27.2 ± 1.1	1.4	3	26.6 ± 1.1	YC1(2+)
CR-3	Vaqueros Fm.	Castle Rock fan	97	26.4 ± 1.4	27.0 ± 0.9	0.6	3	27.0 ± 0.9	0.6	3	27.0 ± 0.9	YC1(2+)
SJB-2	Vaqueros Fm.	Vaqueros Sst.	98	33.8 ± 1.1	84.3 ± 0.8	0.5	6	82.6 ± 0.8	2.4	6	33.8 ± 1.1	YSG
SJB-3	Vaqueros Fm.	Zayante Sst.	148	22.2 ± 0.3	22.3 ± 0.2	0.6	2	22.7 ± 0.1	2.8	5	22.3 ± 0.2	YC1(2+)
AG-1	Temblor Fm.	Agua Sst.	108	24.6 ± 0.8	27.1 ± 0.3	0	2	26.8 ± 0.3	3.8	3	27.1 ± 0.3	YC1(2+)
CRN-1	Temblor Fm.	Carneros fan	98	48.1 ± 1.4	48 ± 1.3	0.1	2	90.7 ± 0.4	1.2	14	NA	NA
CRN-2	Temblor Fm.	Carneros fan	98	44.7 ± 0.7	88.1 ± 0.8	0.8	3	89.2 ± 0.5	1.5	5	NA	NA
CRN-3	Temblor Fm.	Carneros fan	58	25.7 ± 0.6	27.8 ± 0.5	0.2	2	27.0 ± 0.4	4	3	27.8 ± 0.5	YC1(2+)
CRN-4	Temblor Fm.	Carneros fan	59	22.0 ± 0.6	22.7 ± 0.4	1.1	3	22.9 ± 0.3	1.1	4	22.7 ± 0.4	YC1(2+)
CRN-5	Temblor Fm.	Carneros fan	59	25.6 ± 0.7	87.4 ± 0.9	0.3	6	90.1 ± 0.6	2.1	12	25.6 ± 0.7	YSG
CRN-6v	Temblor Fm.	Carneros (Volc.)	60	16.7 ± 0.5	17.3 ± 0.1	0.4	12	17.8 ± 0.1	1.2	23	17.3 ± 0.1	YC1(2+)
CRN-7v	Temblor Fm.	Carneros (Volc.)	98	16.1 ± 0.7	16.6 ± 0.3	0.6	5	17.2 ± 0.2	1.5	11	16.6 ± 0.3	YC1(2+)
WYG-1	Temblor Fm.	Wygal Sst.	110	89.4 ± 1.6	91.0 ± 0.6	0.3	9	92.9 ± 0.4	1.3	20	NA	NA
RP-1	Temblor Fm.	Recruit Pass fan	88	18.4 ± 1.1	18.7 ± 0.7	0.1	3	19.1 ± 0.6	1.4	4	18.7 ± 0.7	YC1(2+)
RP-2	Temblor Fm.	Recruit Pass fan	197	20.4 ± 0.3	22.4 ± 0.2	0.7	3	22.4 ± 0.2	0.7	3	22.4 ± 0.2	YC1(2+)
MC-1	Temblor Fm.	Maricopa fan	99	16.5 ± 0.6	18.3 ± 0.2	0.3	4	17.8 ± 0.2	3.4	3	18.3 ± 0.2	YC1(2+)
PLT-1	Pleito Fm.		99	28.8 ± 0.7	29.3 ± 0.4	0.5	3	29.7 ± 0.3	1.3	4	29.3 ± 0.4	YC1(2+)
TF-1	Temblor Fm.	Lower Temblor	99	23.7 ± 0.5	23.9 ± 0.3	0.4	4	24.2 ± 0.3	1.6	5	23.9 ± 0.3	YC1(2+)
TF-2	Temblor Fm.	Upper Temblor	107	19.3 ± 0.6	19.9 ± 0.2	0.2	8	20.1 ± 0.1	0.7	12	19.9 ± 0.2	YC1(2+)

Note: Coordinates are in World Geodetic System 1984 (WGS84). Fm.—Formation; Sst.—Sandstone; Sh.—Shale; Volc.—volcanics; MSWD—mean square of weighted deviates; NA—not applicable.

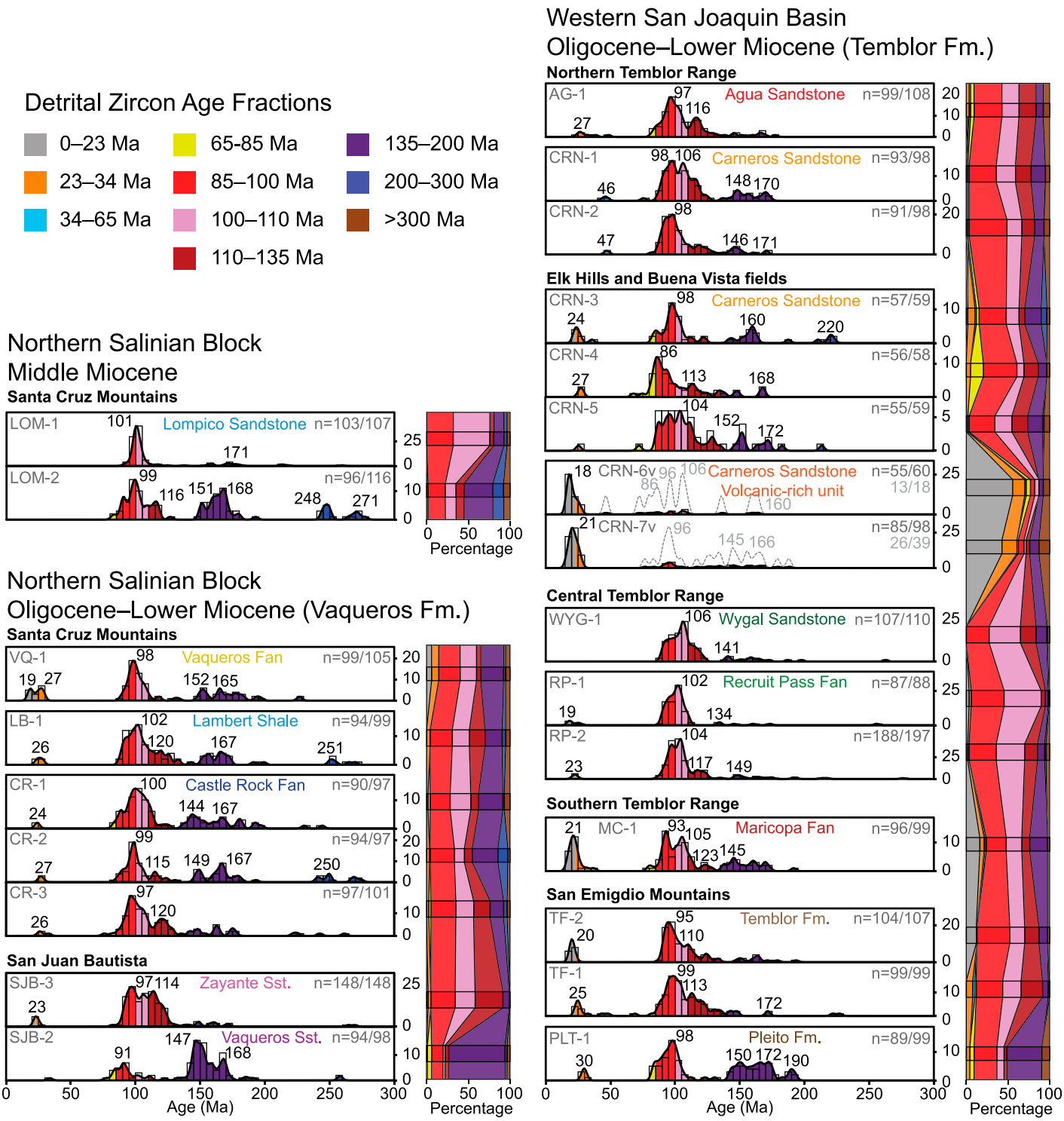

Figure 7. Kernel density estimates (KDEs) and histograms of detrital zircon U-Pb ages for key stratigraphic intervals from Oligocene–Middle Miocene sandstones of the northern Salinian block (left) and western San Joaquin basin (right). See Table 1 for sources of data and Figure 4 for stratigraphic nomenclature. KDEs have a 2 m.y. bandwidth and are colored based on detrital zircon age fractions (see key on top), with peak ages labeled. Numbers of displayed and total grain analyses (*n*) are shown. Dashed gray curves of the two volcanic-rich Carneros Sandstone samples (CRN-6&7v) are KDEs with the Oligocene–Miocene detrital fraction removed. Changes in proportion of detrital zircon age fractions are shown to the right of the KDEs. Sst—Sandstone.

TABLE 3. PROPORTIONS OF DETRITAL ZIRCON AGE FRACTIONS

Sample	Formation	Unit	Grains	Detrital zircon age fractions (Ma)									
				0–23 (%)	23–34 (%)	34–65 (%)	65–85 (%)	85–100 (%)	100–110 (%)	110–135 (%)	135–200 (%)	200–300 (%)	>300 (%)
Middle–Upper Miocene													
LOM-1	Lompico Fm.		107	0	0	0	0	32	44	5	12	4	4
LOM-2	Lompico Fm.		116	0	0	0	2	21	13	9	34	13	8
Oligocene–Lower Miocene													
VQ-1	Vaqueros Fm.	Vaqueros Fan	105	6	9	0	0	26	20	5	28	2	6
LB-1	Lambert Shale	Castle Rock Fan	99	0	4	0	0	26	21	18	20	5	5
CR-1	Vaqueros Fm.	Castle Rock Fan	97	0	2	0	2	24	25	9	29	2	7
CR-2	Vaqueros Fm.	Castle Rock Fan	97	0	3	0	1	29	12	9	31	11	3
CR-3	Vaqueros Fm.	Castle Rock Fan	101	0	3	0	2	30	22	20	16	4	4
SJB-2	Vaqueros Fm.	Vaqueros Sst.	98	0	1	0	5	13	3	4	67	2	4
SJB-3	Vaqueros Fm.	Zayante Sst.	148	1	3	0	1	29	24	33	7	1	0
AG-1	Temblor Fm.	Agua Sst.	108	0	4	2	4	33	20	20	8	0	8
CRN-1	Temblor Fm.	Carneros Fan	98	0	0	2	1	46	17	15	11	0	7
CRN-2	Temblor Fm.	Carneros Fan	98	0	0	2	1	33	23	18	17	0	5
CRN-3	Temblor Fm.	Carneros Fan	59	2	8	2	3	32	15	7	20	7	3
CRN-4	Temblor Fm.	Carneros Fan	58	0	5	0	16	40	9	17	10	0	3
CRN-5	Temblor Fm.	Carneros Fan	59	0	2	0	2	31	20	19	19	2	7
CRN-6v	Temblor Fm.	Carneros (Volc.)	60	55	15	2	5	5	5	0	5	0	8
CRN-7v	Temblor Fm.	Carneros (Volc.)	98	43	17	0	2	7	2	4	11	0	13
WYG-1	Temblor Fm.	Wygal Sst.	110	0	0	0	0	27	37	19	13	1	3
RP-1	Temblor Fm.	Recruit Pass fan	88	3	2	0	0	40	44	5	3	1	1
RP-2	Temblor Fm.	Recruit Pass fan	197	2	1	0	0	32	34	15	9	2	5
MC-1	Temblor Fm.	Maricopa fan	99	16	5	1	2	23	19	9	21	0	3
PLT-1	Pleito Fm.		99	0	4	0	5	27	9	3	41	0	10
TF-1	Temblor Fm.	Lower Temblor	99	0	8	2	2	31	22	25	7	2	0
TF-2	Temblor Fm.	Upper Temblor	107	12	1	0	0	39	18	17	10	0	3
		Gray scale:			0%	10%	20%	30%	40%	50%	60%	70%	

Note: Fm.—Formation; Sst.—Sandstone; Volc.—volcanics.

(34–0 Ma) ages (Table 3). Notably, the Cenozoic age fraction increases northward from the sandstones of the Castle Rock fan to Vaqueros fan (Fig. 7), while Permian to Triassic ages decrease. Cenozoic ages yielded MDAs that matched the previously reported biostratigraphic age constraints of late Oligocene age (Zemorrian stage) for the Castle Rock fan and Lambert Shale units (ca. 27–23 Ma) and an early Miocene age (Saucesian stage) for the Vaqueros fan (ca. 18.6 Ma; Table 2). The distribution of Cretaceous ages was variable throughout the La Honda basin (Fig. 7). The Vaqueros fan (VQ-1) and southernmost samples of the Castle Rock fan (CR-2 and 3) showed peak ages of ca. 99–97 Ma, with the Castle Rock samples including a substantial 100–85 Ma fraction (Table 3). In contrast, the northernmost Castle Rock fan sample (CR-1) and the Lambert Shale (LB-1) showed increased 110–100 Ma ages, with peak ages of ca. 100 and 102 Ma, respectively.

The two middle Miocene (Relizian stage) samples of the Lompico Sandstone showed greater variation than the underlying units. The southern Lompico Sandstone sample (LOM-2; Fig. 4A) had a similar age fraction to the Vaqueros Formation but lacked Cenozoic ages (Fig. 7) and had more abundant Jurassic to Early Cretaceous and Permian to Jurassic fractions. In contrast, the northern sample of the Lompico Sandstone (LOM-1), which is in depositional contact with granitic basement (Fig. 2), showed over 80% Cretaceous ages, with a strong unimodal peak age at ca. 101 Ma.

The Oligocene age (Zemorrian stage) Vaqueros Sandstone at San Juan Bautista (Fig. 2) was notably different than the sandstones of the La Honda basin in that it had a much higher abundance of Jurassic to Early Cretaceous ages (87%; ca. 147 and 168 Ma age peaks). The sample (SJB-2) had additional latest Cretaceous ages with a younger peak age of ca. 91 Ma (Fig. 7). However, the overlying early Miocene age (Saucesian) Zayante Sandstone was substantially different. The Zayante Sandstone sample (SJB-3) yielded over 85% Cretaceous zircon ages that showed peak ages between 114 and 97 Ma. Furthermore, this sample lacked the latest Cretaceous ages present in the underlying Vaqueros Sandstone and had the lowest abundance of Jurassic to Early Cretaceous ages (7%) of all of the samples in the Salinian block.

Western San Joaquin Basin

The detrital zircon age distributions of the Oligocene through Lower Miocene sandstones of the Temblor Formation generally showed similar age fractions as the sandstones of the La Honda basin. Notably, the Permian to Triassic ages (300–200 Ma) that were present in small quantities in the La Honda basin were nearly absent in the San Joaquin basin samples (Table 3). Furthermore, detrital zircon age distributions varied more with latitude than they did with stratigraphic position (Zemorrian vs. Saucesian; Fig. 7). The Agua Sandstone and overlying Carneros Sandstone exposed in the northern Temblor Range (Fig. 2) predominantly showed Late Cretaceous ages (53%–67%; peaks at ca. 97, 98, and 106 Ma) with subordinate quantities of mid-Cretaceous and Jurassic to Early Cretaceous ages. No Oligocene or Miocene ages were found in the Carneros Sandstone of the northern Temblor Range. Both outcrop Carneros Sandstone samples (CRN-1 and 2) had a small fraction of Eocene grains (peaks at ca. 47–46 Ma) that were not found in any of the other Oligocene–Miocene samples (Fig. 7). Eocene source rocks are not present in central California, but Eocene grains of similar age have been reported in the Point of Rocks Sandstone that underlies the Carneros Sandstone in the Temblor Range (Sharman et al., 2013).

Downdip at Elk Hills field (Figs. 2 and 6), the subsurface equivalent of the Carneros Sandstone showed more variable age distributions, including greater abundance of Permian to Early Cretaceous ages (Table 3) and the presence of 2%–9% Oligocene–Miocene ages (MDAs of 26–22 Ma). Peak Cretaceous ages ranged ca. 86, 98, and 104 Ma in these three samples (CRN-3, 4, and 5), respectively (Fig. 7). Further basinward, the two samples (CRN-6v and 7v) of volcanic-rich sandstone were dominated by Miocene and Oligocene ages (up to 55% and 17%, respectively). These units were associated with the Carneros Sandstone based on general stratigraphic subsurface correlation (Fig. 4B), and MDAs of 16.6 and 17.3 Ma (YC1σ2+) suggest that the volcanic-rich sandstone was deposited at the very end of the early Miocene or later. Additionally, these samples had the highest proportion of pre-Permian ages (>300 Ma) in this study (8% and 13%; Table 3).

The Oligocene Wygal Sandstone and younger Recruit Pass fan of the central Temblor Range showed similar age distributions dominated by mid- to Late Cretaceous ages (>80%), and

specifically showed the highest abundance of 110–100 Ma ages in this study (34%–44%). The peak age for the Wygal Sandstone is ca. 106 Ma, and the two Recruit Pass samples (RP-1 and 2) had peak ages of ca. 102 and 104 Ma, respectively (Fig. 7). Furthermore, the Recruit Pass fan sandstones had low proportions of pre- and post-Cretaceous zircon (Table 3), the latter of which yielded MDAs of ca. 19 and 22 Ma (YC1σ2+; Table 2). Previously, the Recruit Pass fan was generally assigned to late Zemorrian or Saucesian age (ca. 28–16.5 Ma) based on foraminiferal samples (Graham et al., 1989). The base of the sandstone is not exposed, but samples were taken from the lower and upper portions of the outcrop (Fig. 4), and the new MDAs constrain most of the Recruit Pass fan deposition to have occurred during the Saucesian or later.

With the exception of the volcanic-rich Carneros Sandstone, the southern Temblor units had the greatest abundance of Cenozoic ages (Table 3). The Lower Miocene Maricopa fan in the southern Temblor Range had ~21% Cenozoic ages that yielded a preferred YC1σ2+ MDA of ca. 18 Ma (Table 2). Additionally, the Maricopa fan had higher abundances of Jurassic to Early Cretaceous ages (21%) than the sandstones to the north and had Cretaceous age peaks at ca. 93 and 105 Ma. In the San Emigdio Mountains (Fig. 6), the Lower Oligocene Pleito Formation had two distinct dominant age fractions: Late Cretaceous and Jurassic to Early Cretaceous (Fig. 7). Conversely, the overlying Temblor Formation samples (Zemorrian and Saucesian stage; TF-1 and TF-2) gave less abundant Jurassic to Early Cretaceous ages, significantly more mid- to Late Cretaceous ages than the Pleito Formation (Table 3; Fig. 7), and greater than 8% Cenozoic ages (YC1σ2+ MDAs of ca. 24 and 19 Ma).

Detrital Zircon Th/U Ratios

In a survey of detrital zircons of the North American Cordillera, McKay et al. (2018)

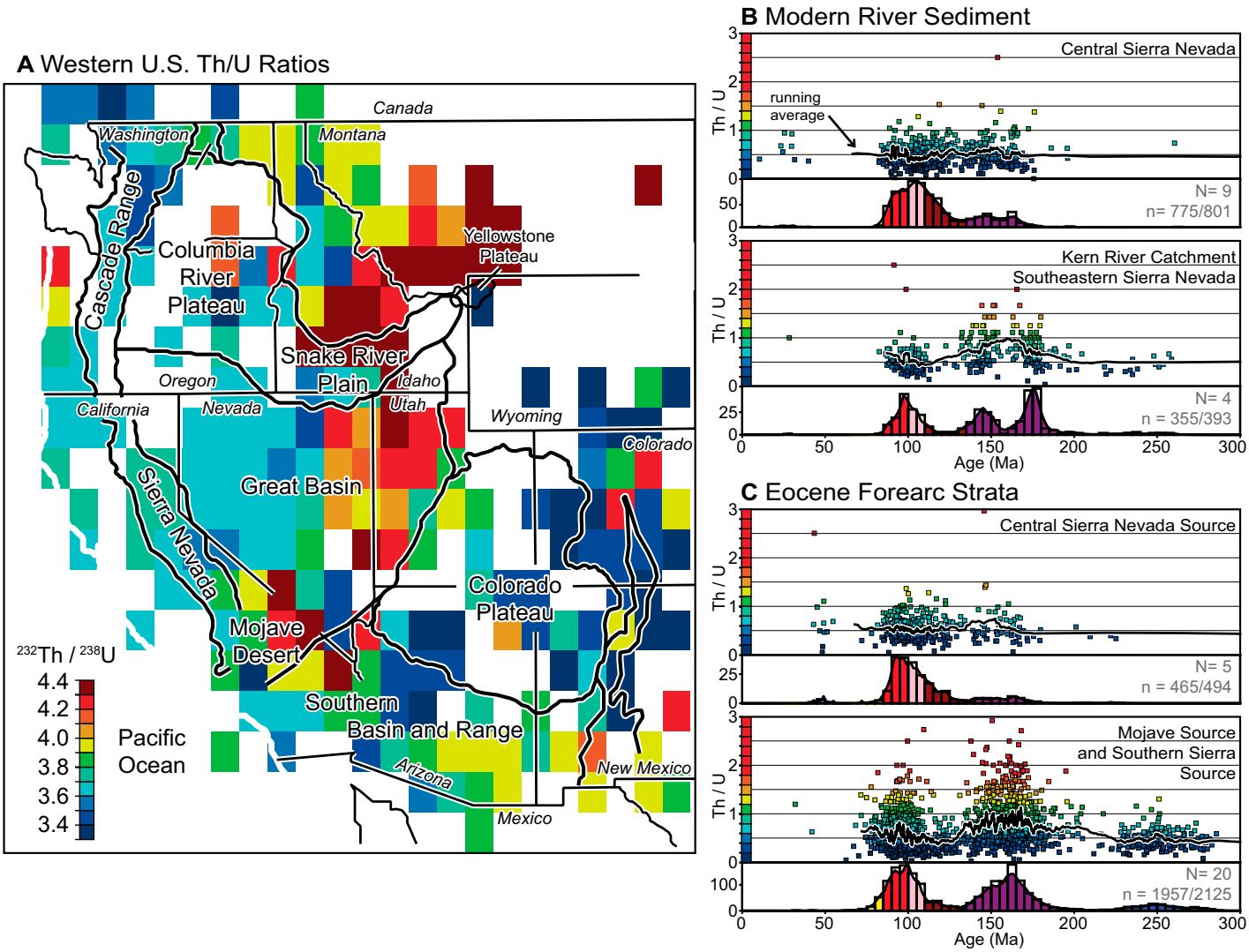

Figure 8. (A) Map of 97.5 percentile grid cell (1° × 1°) averages of time-integrated Th/U ratios (modified from Bouchet et al., 2014) calculated from Pb isotopic data of a combined data set from ores, K-feldspars from felsic plutonic rocks, and felsic plutonic whole rocks. (B) Detrital zircon U-Pb data and zircon Th/U ratios from modern rivers with watersheds in the central and southeastern Sierra Nevada batholith (data from Malkowski et al., 2019; Saleeby et al., 2016). (C) Eocene forearc strata interpreted to have a central Sierra Nevada source and a western Mojave–southern Sierran source (data compiled by Sharman et al., 2015). See Supplementary Table S5 (see text footnote 1) for sample sources and locations. Note that the range in values for color scales of whole bedrock Th/U and detrital zircon Th/U are not the same.

observed that zircon produced by melts associated with extensional magmatism contains variable Th/U, including significant higher fractions (>1.0), whereas melts associated with compressional magmatism are less variable with low Th/U (<1.0). Furthermore, Bouchet et al. (2014) compiled a database of Pb isotope compositions from basement ores, K-feldspars, and felsic whole-rock samples for the western United States and converted the data set into modeled $^{232}Th/^{238}U$ ratios (Fig. 8A). They found a spatial trend of high Th/U values from the Snake River basin, across the eastern Great Basin, and into the Mojave and Yavapai blocks (Figs. 1 and 8). Conversely, the lowest Th/U values were observed in more westward areas dominated by younger basement ages (e.g., western Great Basin, Sierra Nevada, Peninsular Ranges, Salinian block, Klamath Mountains, Cascade Ranges, and Columbia River and Colorado Plateaus).

Sharman et al. (2018) noted that the Th/U ratios in Mesozoic detrital zircon of the California forearc basin, specifically Jurassic to Early Cretaceous age fractions (200–135 Ma), were systematically higher (>0.6 mean) for sandstone with inferred southern Sierra Nevada and northwestern Mojave Desert provenance (i.e., Butano Sandstone), relative to those with Sierra Nevada batholith provenance (i.e., Point of Rock Sandstone; ~0.6 mean). Figure 8C shows published detrital zircon U-Pb and Th/U data for all Eocene sandstone of the California forearc with inferred central Sierra Nevada and Mojave–southern Sierran sources (Sharman et al., 2015). Furthermore, published detrital zircon U-Pb data from modern rivers with headwaters in the central Sierra Nevada batholith, southeastern Sierra Nevada (Kern River drainage), and Jurassic plutons southeast of the Sierra Nevada batholith (Lechler and Niemi, 2011; Niemi, 2013; Malkowski et al., 2019) provide the best proxy for ages and Th/U values of the source regions (Fig. 8C). Zircon grains derived from the central Sierra Nevada batholith have few Th/U values higher than 1.0 (<3%), with mean values of ~0.5 and 0.6 for Cretaceous and Jurassic zircon, respectively. In contrast, zircon grains derived from the Mojave and southern Sierra Nevada have a greater abundance of Th/U values higher than 1.0 (>13%), with mean values of 0.6–0.7 and 0.8–0.9 for Cretaceous and Jurassic zircon, respectively.

The range in Th/U values for detrital zircon (~0–4) differs from the range for modeled whole-rock Th/U values (~3.4–4.4; Bouchet et al., 2014) because U and Th are preferentially incorporated into minerals at different proportions as they crystallize out of melt. It should be noted that U and Th content in minerals will depend on the order of crystallization, and therefore the chemical composition of an accessory mineral does not have a simple proportional relationship with the chemistry of the magma (Breiter, 2016). However, the trends in Th/U distributions for modern river sediment and the Eocene sandstones of the California forearc match remarkably well with the spatial trends of their inferred basement source regions (Figs. 8A–8C; Bouchet et al., 2014). Because basement source areas for central California share similar U-Pb age fractions, and because provenance interpretations of detrital zircon samples are mostly based on relative abundances of these fractions, we used the detrital zircon Th/U to further discriminate among sources of similar age. This approach has successful been used by Riggs et al. (2013, 2020) to discern between similar age populations in the early Mesozoic Cordilleran arc. For each Oligocene–Lower Miocene depositional system of the San Joaquin and northern Salinian block, we compiled Th/U values by Jurassic to Early Cretaceous (group J; 200–125 Ma), mid- to Late Cretaceous (group K; 125–65 Ma), and Cenozoic (group CZ; 65–0 Ma) U-Pb age fractions and present the distribution (KDE) and mean and median values for each age group in Figure 9.

Mesozoic (200–65 Ma) Detrital Zircon Th/U Values

The distribution of Th/U ratios for zircon grains in groups K and J of the Oligocene–Lower Miocene Temblor and Vaqueros Formations had few variations with stratigraphic age but was spatially diverse. Sandstones of the La Honda basin (Fig. 9, top) had among the largest range (wide distributions) and highest Th/U values in this study. Mean Th/U values for group K and J zircon grains were highest in the northern Vaqueros fan (1.0 and 1.2, respectively), with values as high as ~3.0. There was a slight southward trend in decreasing values across the basin, with mean group K and J values of 0.5 and 0.9, respectively, in the Castle Rock fan. South of the La Honda basin, the sandstones of the San Juan Bautista area (Fig. 2) showed variable Th/U ratios. The Vaqueros Sandstone continued to have high group K and J values (mean 0.6 and 1.0), but the overlying Zayante Sandstone had the lowest values of samples from the Salinian block (0.4 and 0.5, respectively; Fig. 9).

The Upper Oligocene to Lower Miocene (Zemorrian–Saucesian) Temblor Formation sandstones of the western San Joaquin basin (Fig. 9, bottom) showed a distinct northwest to southeast increase in mean Th/U of both group K and J zircon grains, with the greatest difference at the spatial transition from central to southern Temblor Range. Sandstones of the northern Temblor Range had few Th/U values greater than 1.0, with mean values restricted to 0.4–0.7 for both groups, although the highest mean value (Agua Sandstone, group J) only had a small sampling of 11 zircon grains and may not have been statistically robust (Fig. 9). The Wygal Sandstone and Recruit Pass fan of the central Temblor Range showed the lowest values in the western San Joaquin basin. To the southeast, the volcanic-rich sandstones that interfinger with the Carneros fan (see Fig. 6) were abruptly high in Th/U relative to their updip counterpart. The Maricopa submarine fan of the southern Temblor Range and the Temblor Formation of the San Emigdio Mountains showed slightly higher Th/U group K zircon values (mean 0.5) than the northern sandstones, but significantly higher group J values (mean 0.8–0.9). The Lower Oligocene Pleito Formation, which underlies the Temblor Formation in the southern San Joaquin basin (Fig. 4B), had the greatest range of values in the basin (~3.0) and highest mean Th/U for group K and J zircon values (0.7 and 1.1, respectively; Fig. 9).

Cenozoic (65–0 Ma) Detrital Zircon Th/U Values

The distribution of Th/U in the young, near-contemporaneous zircon grains of group CZ was highly variable throughout the study area (Fig. 9). For example, whereas the updip Carneros Sandstone of the northern Temblor Range had a mean value of 0.6, the downdip volcanic-rich deposits had the greatest range (up to ~3.5), with few zircon values less than 0.5 and a mean Th/U value of 1.2 (Fig. 9). The group CZ zircon grains of the La Honda basin (northern Salinian block) and the Temblor Range (San Joaquin basin) all had mean Th/U values greater than 0.6, with the Vaqueros fan, Agua Sandstone, and Maricopa fan exceeding a mean of 1.0 (Fig. 9). In contrast, the few group CZ zircon grains present in the southernmost Temblor Formation–age sandstones (San Juan Bautista region and San Emigdio Mountains) showed the lowest values (mean <0.5).

SANDSTONE PROVENANCE

Potential Sediment Sources

The plutonic, volcanic, metamorphic, and sedimentary rocks that were possible sources of local and extraregional sediment to the central California margin during the Cenozoic have been discussed at length in recent studies (Sharman et al., 2015; Gooley et al., 2020). These include northerly sources (i.e., Idaho batholith, Cenozoic volcanism in the Great Basin, and Klamath Mountains), sources adjacent to the San Joaquin basin (i.e., granitic basement of the Sierra Nevada batholith, Salinian block, and Mojave

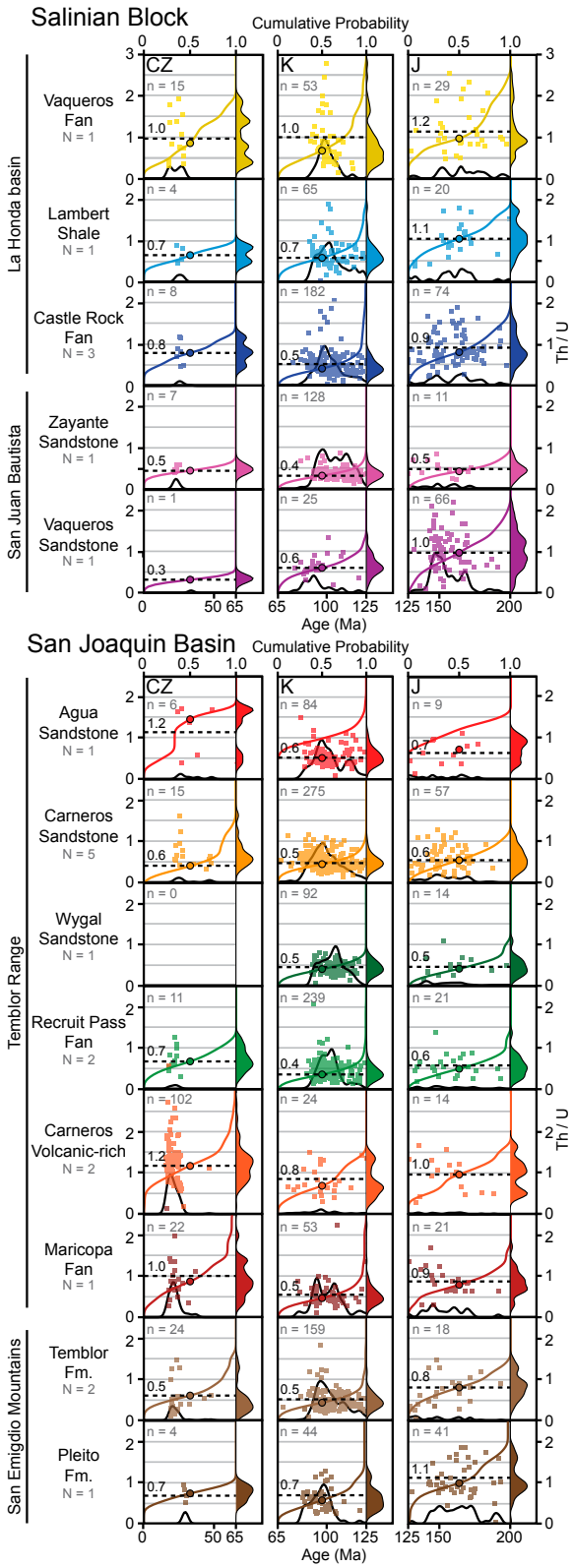

Figure 9. Detrital zircon Th/U vs. U-Pb age for Oligocene–Lower Miocene sandstone samples of the northern Salinian block and western San Joaquin basin. Age fractions are divided by Cenozoic (CZ; 0–65 Ma), mid–Late Cretaceous (K; 65–125 Ma), and Jurassic–Early Cretaceous (J; 125–200 Ma). Black line is the kernel density estimate (KDE) of the U-Pb ages, and colored line is the cumulative distributions plot (CDP) of Th/U, with the corresponding KDE shown on the right *y* axis. The median Th/U ratio for each distribution is shown as a circle on the CDP at 0.5, and the mean Th/U ratio is denoted by a dashed line with the value labeled above. Numbers of samples (*N*) and analyses in each plot (*n*) are annotated. Note that a single value >3.0 in the Carneros volcanic-rich sandstone and a single value >2.5 in the Maricopa fan (group CZ) extend into the overlying chart.

Desert; Fig. 1), and intrabasinal sources (local Cenozoic volcanism and the underlying stratigraphy). While all of these are considered as possible sources of sediment, the latter adjacent and local sources are considered the most plausible source areas for the western San Joaquin basin and northern Salinian block. In addition, we compared our data to the Eocene stratigraphy that was derived from the Sierra Nevada batholith and Mojave Desert sources (e.g., Sharman et al., 2013, 2015) to demonstrate changing sediment source areas.

Detrital Zircon Provenance

A comparison of the detrital zircon age fractions of Eocene through Lower Miocene sandstones of the northern Salinian block and western San Joaquin basin showed that mixing of Sierra Nevada and southern Sierran and Mojave zircon occurred as new and recycled sediment sources were redistributed across the basin. Ternary mixture diagrams of the relative proportions of zircon ages most similar to southern Sierran and western Mojave sources (>135 Ma) with ages representative of the Early (135–100 Ma) and Late (100–65 Ma) Cretaceous magmatic arc show a clear distinction between the Sierra Nevada batholith–derived Eocene Point of Rocks Sandstone and the Mojave–southern Sierran–sourced Butano Sandstone and Tejon Formation (Figs. 4 and 10A). The Oligocene–Lower Miocene sandstones show variability in this ternary space relative to the Eocene fields. The Early and Late Cretaceous age groups are also present in the Salinian basement rocks of Montara Mountain and the northern Gabilan Range (135–100 Ma), and Ben Lomond and southern Gabilan Range (100–65 Ma; Fig. 2).

Additionally, a nonmetric MDS comparison of statistical similarities of Oligocene to Lower Miocene Salinian and San Joaquin basin samples with the underlying Eocene sandstones can be used to infer sediment mixing trends between two distinct fields: central Cretaceous Sierran Nevada batholith and Mojave–southern Sierran (Fig. 10B). Since our samples have contemporaneous ages (e.g., Oligocene–Miocene volcanics) that were not available as sources of zircon for older samples, we removed all late Cenozoic (<34 Ma) zircon ages from this first MDS plot. Samples that clustered closely were interpreted to share a similar sediment source, while outliers may have had additional sources or an abundance of a single fraction (e.g., distinct plutonic ages). However, in a second plot (Fig. 10C), we compared only Oligocene through Lower Miocene sandstones and included all zircon ages. By comparing these plots, we can discern whether younger source fractions affected the statistical comparison of pre-Cenozoic basement sources.

Northern Salinian Block Provenance

The Vaqueros Formation sandstones of the La Honda basin share some similarities in detrital age distributions with the underlying Butano

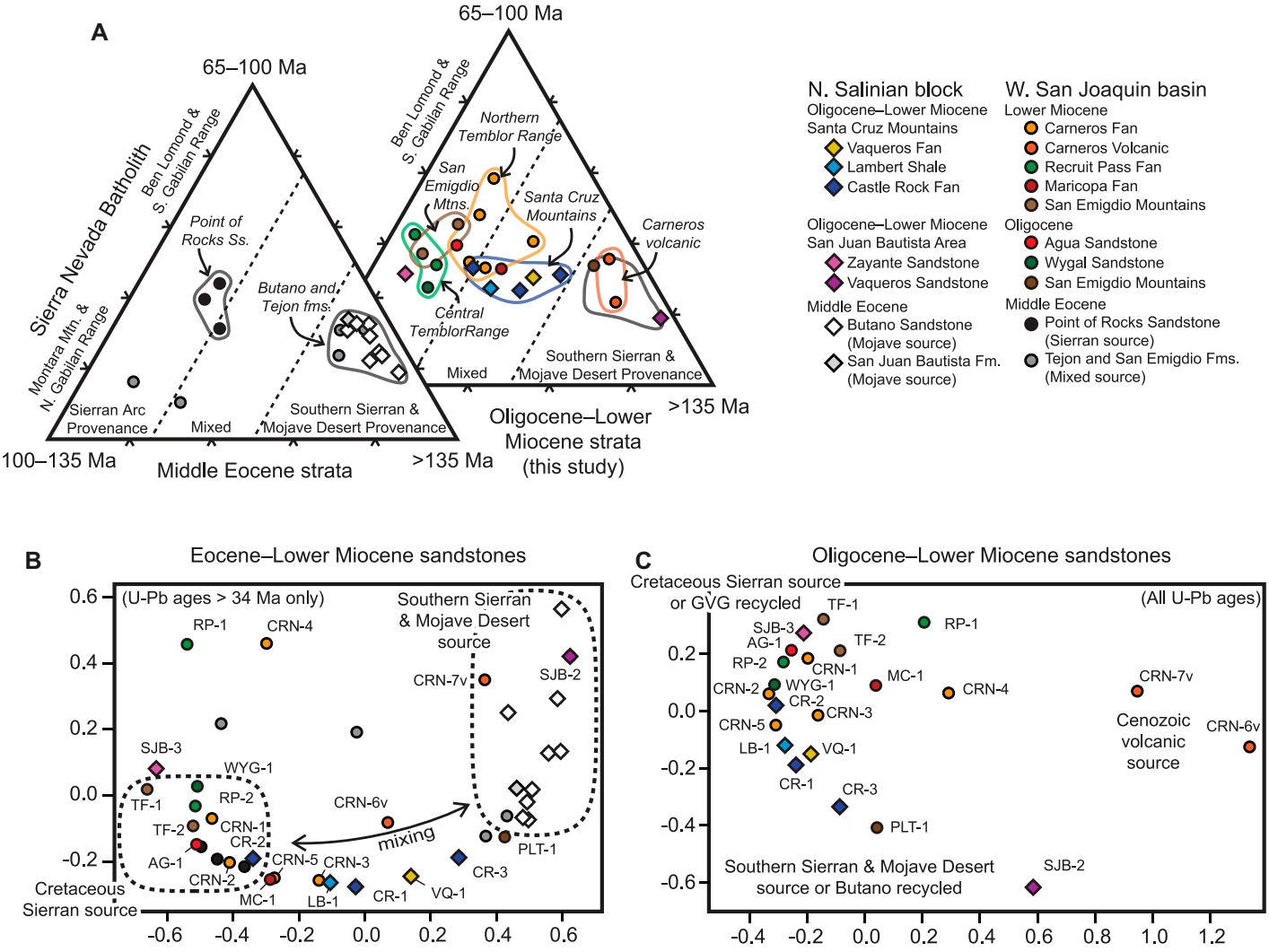

Figure 10. Detrital mode and provenance mixing relationships in sandstones of the northern Salinian block (La Honda basin) and western San Joaquin basin. (A) Ternary diagram of Cretaceous (65–100 and 100–135 Ma) and Jurassic–Precambrian (>135 Ma) U-Pb detrital zircon ages for Middle Eocene (left) and Oligocene–Lower Miocene (right) sandstones of the southwestern San Joaquin basin and northern Salinian block. Fields that encompass the Middle Eocene strata (gray) are projected to the right plot for comparison. (B) Dimensionless nonmetric multidimensional scaling (MDS) plot of detrital zircon U-Pb age distributions for Eocene and Oligocene–Lower Miocene sandstone samples. Late Cenozoic zircon ages (<34 Ma) were excluded from the MDS transformation in order to compare basement sources. Provenance fields are indicated with mixing trends between sources. (C) MDS plot of Oligocene–Lower Miocene sandstone samples including all zircon ages. GVG—Great Valley Group; Ss—Sandstone.

Formation. Elevated Jurassic–Early Cretaceous age fractions with high Th/U values were likely originally derived from the western Mojave Desert and/or southern Sierra Nevada batholith (Figs. 2 and 9). However, the increased abundance of Cretaceous zircon in the Vaqueros Formation relative to the Eocene Butano Sandstone suggests increased contributions from a mid-Cretaceous granitic source. Specifically, we interpret variations in the peak Cretaceous ages (Fig. 7) to reflect exhumation and erosion of the Ben Lomond and Montara Mountain granitic basement of the northern Salinian block (Stanley, 1985; Graham et al., 1989). Furthermore, petrologic evidence of Franciscan detritus (e.g., radiolarian chert) contributing to the Vaqueros submarine fan sandstone indicates that secondary recycling of subduction complex and older Paleogene strata occurred. Therefore, the Mojave and southern Sierran sediment was likely recycled into the Oligocene–Lower Miocene sandstones from Paleogene strata (e.g., Butano Sandstone) exhumed from the adjacent hinterland.

MDS and ternary mixing relationships support the inference that the sandstones of the Vaqueros fan, Castle Rock fan, and Lambert Shale represent mixtures of recycled Mojave–southern Sierran detritus with a Cretaceous igneous source (Fig. 10). The southern Lompico Sandstone of the La Honda basin shares similar age fractions with the Butano Sandstone, including elevated Permian through Early Cretaceous age fractions originally derived from a Mojave–southeastern Sierran source. This relationship likely reflects recycling directly from the older forearc deposits of the southern La Honda basin (Fig. 1). Conversely, the northern Lompico Sandstone sample directly onlaps the granitic basement of Montara Mountain, and the unimodal Cretaceous age peak (ca. 101 Ma) likely is the most informative representation of the U-Pb age of the

southern side of the Montara Mountain tonalite (Figs. 2 and 7). In comparison, the modern San Lorenzo River catchment consists of southern La Honda basin Cenozoic stratigraphy and the Ben Lomond granodiorite. The U-Pb age distribution from modern San Lorenzo River sediment (Sickmann et al., 2016) has a Cretaceous age peak (ca. 98 Ma) likely representative of Salinian granites of the southern La Honda basin and has age fractions similar to those of the southern Castle Rock fan samples (i.e., CR-2 and 3; Fig. 7).

The detrital zircon age distributions of the Vaqueros Formation of San Juan Bautista are similar to the Eocene Butano Sandstone and San Juan Bautista Formation (Figs. 4A and 10A). Mixing trends show that this sandstone (SJB-2) is unlikely to have received a sediment contribution from the Cretaceous Sierra Nevada batholith or Salinian block (Figs. 10B and 10C), and it is evident that Mojave and southern Sierra detritus continued to be routed to the area south of the La Honda basin through the Oligocene. However, the overlying Zayante Sandstone (SJB-3) shows an abrupt transition to principally Cretaceous granitic sources (Fig. 7). This likely reflects early uplift of northern Gabilan Range granites along the Zayante fault (Fig. 2; Clark and Rietman, 1973; Stanley, 1985).

Western San Joaquin Basin Provenance

The sandstones of the western San Joaquin basin demonstrate inconsistent and variable age distributions from north to south; however, samples of Oligocene and early Miocene age are generally similar within local geographic regions (Fig. 7), and we infer that this is due to latitudinal changes in sediment provenance. The sandstones of the northern Temblor Range (Agua and Carneros) have U-Pb age distributions and Th/U ratios (Fig. 9) that were likely originally sourced from the Sierra Nevada batholith and were subsequently recycled from the Franciscan subduction complex and Great Valley forearc strata (Fig. 10) exposed in the emergent Temblor Range and southern Diablo Range. This interpretation is supported by reported Franciscan detritus and facies relations culminating in alluvial deposits in the northwest Carneros Sandstone (e.g., Pence, 1985; Graham et al., 1989). The shift in Cretaceous age peaks in the Carneros Sandstone sample of Elk Hills relative to outcrop samples (Fig. 7) may be the product of stratigraphic unroofing and sediment recycling of Cretaceous through Eocene strata that recorded an evolving Cretaceous magmatic arc. Alternatively, the increased abundance of 110–100 Ma ages (e.g., CRN-5; Fig. 7) could have been contributed by the northernmost Salinian basement, west of the San Andreas fault. The differing lithology, U-Pb ages, Th/U ratios, and relatively young MDAs (ca. 17–16 Ma) of volcanic-rich sandstone at Elk Hills and Buena Vista suggest that this unit is distinct from the proper Carneros Sandstone and rather is an interfingering or overlying unit rather than a downdip depositional counterpart.

The central Temblor Range Oligocene Wygal Sandstone and sandstones of the Recruit Pass submarine fan have significantly fewer pre-Cretaceous ages than those found in Oligocene–Lower Miocene sandstone throughout the rest of the western and central San Joaquin basin (Fig. 7) and demarcate the lowest Th/U values for group K and J zircon in the basin (Fig. 9). These samples fall within the Cretaceous Sierran source fields or are entirely distinct from other samples on the MDS plots (Figs. 10B and 10C) and are well into the Sierran arc sources in ternary space (Fig. 10A). The minor pre-Cretaceous ages in the shallow-marine Wygal Sandstone (Fig. 7), unconformable relationship with underlying Eocene strata (Fig. 4B), and reported pebbles from the Great Valley Group (Bent, 1985; Carter, 1985) demonstrate that sediment recycling off the southern Diablo Range likely occurred. However, a Cretaceous source of sediment with ages ca. 106–102 Ma was directly available to the central Temblor Range and, by the time of Recruit Pass fan deposition, was not diluted by detrital age distributions that are found throughout much of the basin.

During Eocene time, the southern San Joaquin basin had an introduction of sediment derived from the southern Sierran and Mojave Desert (Sharman et al., 2015). This is demonstrated by the presence of pre-Cretaceous zircon in the Tejon and San Emigdio Formations (Fig. 10A). Shulaker et al. (2019) documented a reduction in drainage area of this source region by early Miocene time by comparing changes in Pb isotopic compositions of K-feldspar in Lower Eocene and Lower Miocene strata to igneous basement sources. The U-Pb age distributions of the Oligocene–Lower Miocene sandstones in the San Emigdio Mountains and southern Temblor Range further constrain the timing of drainage reorganization in the San Joaquin basin. This is supported by the presence of Jurassic age fractions and specifically group J zircon grains with high Th/U values (Fig. 9), which are common in sediment sourced from the Mojave region (e.g., Butano Sandstone; Fig. 8). Specifically, the transition from the Pleito Formation to the Temblor Formation in the San Emigdio Mountains (samples PLT-1 to TF-1 in Figs. 4B, 7, and 10) demonstrates a switch from a primary extraregional Mojave source to a local Sierra Nevada batholith source by the end of Oligocene time (MDA of ca. 23.9 Ma; Table 2). To the north, in the southern Temblor Range, the younger Lower Miocene Maricopa fan received a mixture of these sources (Fig. 10), likely recycled from exhumed Eocene strata from the southwest, with an additional source of ca. 21 Ma volcanic detritus. This latter switch in provenance constrains the timing of redistribution of southern Sierran– and Mojave-sourced sediment into the southern San Joaquin basin to around 18 Ma or earlier (Table 2).

Sources of Cenozoic (30–18 Ma) Zircon in Central California

With the exception of the ca. 23 Ma Pinnacles-Neenach volcanic complex, late Oligocene volcanic rocks with ages of ca. 30–24 Ma are rare throughout central California (Stanley et al., 2000). However, an Upper Oligocene–Lower Miocene unit of fluvially reworked rhyolitic volcanic detritus (i.e., Valley Springs Formation) is widespread to the north throughout the Sacramento and northern San Joaquin basin (Bartow, 1992). Stratigraphic and sedimentological evidence shows that the volcanic sediment was derived from eruptive centers in the Great Basin (Nevada caldera complex; Fig. 1) and transported across the Sierra Nevada through paleovalleys (Henry and Faulds, 2010; Henry et al., 2012; Wakabayashi, 2013). Furthermore, detrital zircon U-Pb ages from correlative units in the southwestern Sacramento basin (Fig. 1; Gooley et al., 2020) show a ca. 27–23 Ma age fraction (ca. 24 Ma peak) that corresponded to felsic volcanism of the Nevada caldera belt (Fig. 1). Southward fluvial transport into the San Joaquin basin occurred during late Oligocene–early Miocene time (Bartow, 1991), and it is likely that Oligocene age fractions present in the Carneros Sandstone were reworked from the Valley Springs Formation and distributed along the western margin of the basin through shallow-marine mixing of sediment. However, the source of >24 Ma Oligocene age fractions in southern San Joaquin basin (San Emigdio Mountains) and the La Honda basin is less clear. These ages possibly represent earlier phases of volcanism than previously recognized in the volcanic centers of central California (e.g., Pinnacles-Neenach, Mindego volcanics) associated with the development of the transform margin. Alternatively, Great Basin volcaniclastic sediment may have circumvented the southern Sierra Nevada and supplied the southernmost San Joaquin basin and northern Salinian block.

Late Oligocene–early Miocene volcanic rocks (ca. 28–22 Ma) in central California include the Mindego volcanic center of the Santa Cruz Mountains, Zayante volcanics of the northern Gabilan Range, and the Tecuya and Tunis volcanics in southern San Emigdio Mountains (Fig. 2;

Stanley, 1990). Reid (1995) suggested that volcanic vents associated with the Mindego Basalt (La Honda basin) were the most likely source of early Miocene volcanic detritus in the western San Joaquin basin center. In concurrence, the high Th/U early Miocene age fractions (Fig. 9) in the similar-age Vaqueros fan (La Honda basin) and Maricopa fan (southern Temblor Range) were likely derived from an intermediate–mafic volcanic source (e.g., the Mindego volcanic center). More specifically, the very high Th/U volcanic-rich Carneros Sandstone unit of the Buena Vista and Elk Hills fields could possibly have been associated with a younger phase of increased volcanism from the Mindego volcanic complex that shed eastward into the San Joaquin basin. Conversely, the relatively lower Th/U early Miocene age fractions found in the San Emigdio Mountains (Figs. 7 and 9) were likely sourced from the updip Tecuya volcanics to the southeast (Fig. 4B).

Sources of Late Cretaceous (110–100 Ma) Zircon to the Central Temblor Range

The dominantly Cretaceous U-Pb age distribution of the Temblor Formation sandstones at Recruit Pass requires a source of exclusively Cretaceous-age detritus (ca. 106–102 Ma) to have been in close proximity to the central Temblor Range. A possible source of 110–100 Ma sediment was the southern Sierra Nevada batholith (east of Bakersfield, Fig. 2). However, eastward-trending paleocurrents in the Recruit Pass fan (Carter, 1985; Graham et al., 1989), the position of the central Temblor Range on the western paleobathymetric slope of the Zemorrian–Saucesian stage San Joaquin basin (Bandy and Arnal, 1969), and presence of adjacent coeval sandstones with diverse age distributions (Fig. 9) make it highly implausible for 110–100 Ma Sierra Nevada detritus to have circumvented the entire San Joaquin basin and been deposited uniquely in the central Temblor Range.

Alternatively, 110–100 Ma granite of the Salinian block is currently exposed at Montara Mountain and the northern Gabilan Range (Fig. 2). The northern side of Montara Mountain has been radiometrically dated with zircon U-Pb ages of ca. 104–102 Ma (Mattinson, 1994; Kistler and Champion, 2001). Furthermore, the detrital ages from the Middle Miocene Lompico Sandstone, which directly onlaps Salinian basement, suggest that the southern side of Montara Mountain yields ca. 101 Ma zircon. Therefore, the granite of Montara Mountain was a likely source of detrital zircon for the Recruit Pass fan. The age of the granitic basement north of Montara Mountain is unconstrained, as the northernmost Salinian block has been translated northward along the San Gregorio–Hosgri fault and is presently submerged in the Pacific Ocean (Fig. 1).

SAN ANDREAS FAULT SLIP HISTORY

Cross-Fault Relationships of the Salinian Block and San Joaquin Basins

A comparison of the detrital zircon age distributions from Oligocene–Lower Miocene submarine fan systems of Graham et al. (1989) demonstrate (Fig. 6) that the Recruit Pass submarine fan of the Temblor Formation does not share a common provenance with the Castle Rock fan, Lambert Shale, or other Vaqueros Formation sandstones (Fig. 11). Furthermore, based on our MDAs (Table 2), the Recruit Pass fan is likely to have been primarily deposited during the Saucesian (early Miocene), whereas the Castle Rock fan is primarily Zemorrian (late Oligocene; Fig. 4). These data challenge the hypothesized contiguous Castle Rock–Recruit Pass submarine fan system across the trace of the San Andreas fault (e.g., Graham et al., 1989; Fig. 6). While this alone does not preclude the two depositional systems from having been adjacent across the fault, we propose that the provenance relationships of Oligocene–Lower Miocene sandstones throughout the northern Salinian block and western San Joaquin basin can be best resolved by aligning the northern Salinian basement (e.g., Montara Mountain) adjacent to the central Temblor Range (Fig. 12). Some researchers (Champion, 1989; Champion and Kistler, 1991) have invoked a pre–5 Ma segment of the San Gregorio–Hosgri fault that dextrally translated Montara Mountain ~40–80 km northward from an original position next to Ben Lomond, based on alignment of a steep gradient in basement Sr initial values. However, there is no independent evidence of significant strike-slip displacement along faults in the La Honda basin, and the differing zircon U-Pb ages of the Montara Mountain (ca. 104–102 Ma) and Ben Lomond (ca. 99–91 Ma; Kistler and Champion, 2001) basement do not support this correlation.

A solution that aligns the northern Salinian basement adjacent to the Temblor Range is appealing because it: (1) juxtaposes a source of ca. 104–101 Ma granitic basement next to the Wygal and Recruit Pass sandstones; (2) aligns the high Th/U southern Sierran and Mojave-derived sediment that was redistributed into sandstones of the La Honda basin with the similar Maricopa fan and Temblor Formation of the San Emigdio Mountains; and (3) aligns mafic to intermediate volcanics of the Mindego volcanic center so that it could have possibly supplied the high Th/U volcanic zircon that is prevalent in the Maricopa fan and volcanic-rich distal Carneros Sandstone (Fig. 12).

Reconciling Variable Displacement of Coeval Features

Restoration of the Montara Mountain granite of the northern Salinian block to a position adjacent to the central Temblor Range (Fig. 12) requires at least 360 ± 15 km of post–early Miocene (ca. 16 Ma) right-lateral displacement of the Salinian block. The uncertainty in displacement magnitude is estimated by considering the reported width of the Recruit Pass fan (~30 km; Graham et al., 1989). Slip displacement along the San Andreas fault greater than 360 km is possible if the Salinian granite north of Montara Mountain were the source of sediment for the Recruit Pass fan. When this slip magnitude is palinspastically restored (Fig. 12), it presents an apparent misalignment of other previously accepted cross-fault ties (Fig. 6), including the early Miocene shoreline and volcanic rocks of San Juan Bautista and the San Emigdio Mountains (Fig. 4; Dickinson et al., 1972), the late Oligocene and early Miocene paleobathymetry on the southern margin of the La Honda and San Joaquin basins (Stanley, 1987), and, most notably, the approximate 315 km of offset on the

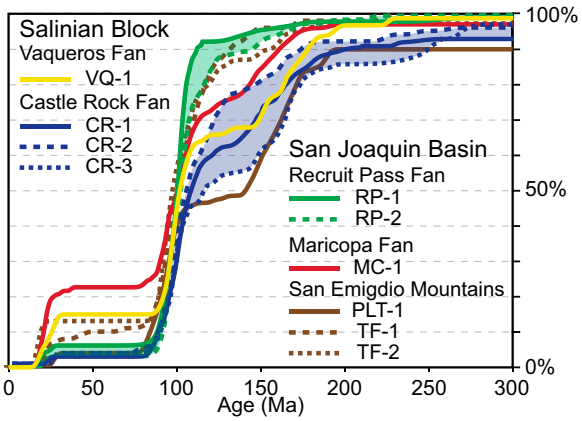

Figure 11. Cumulative distribution function of detrital zircon U-Pb age distributions from Oligocene–Lower Miocene sandstones of the northern Salinian block and western San Joaquin basin.

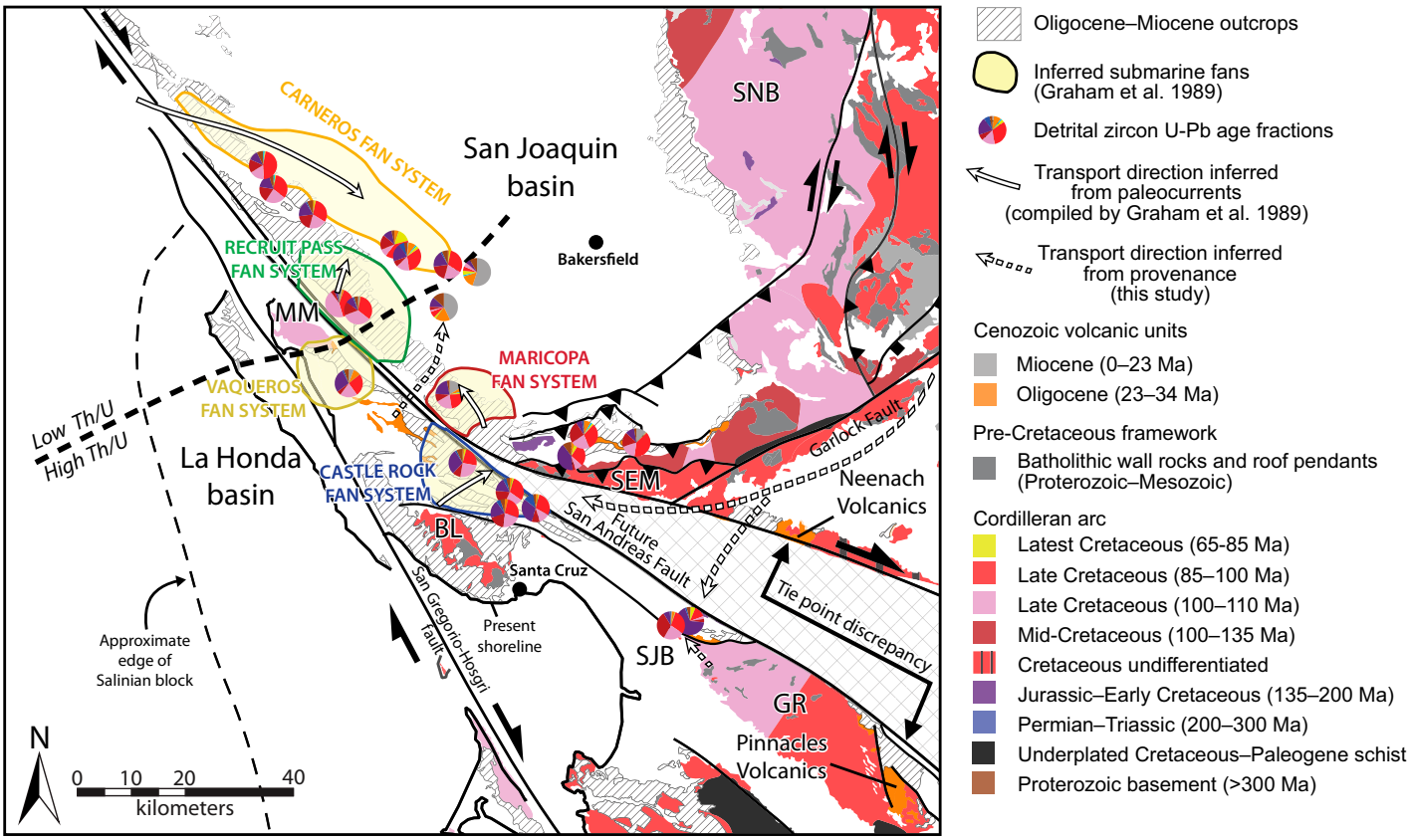

Figure 12. Alignment of sediment dispersal systems in the northern Salinian block and western San Joaquin basin during late Oligocene–early Miocene time (compare with previous interpretation shown in Fig. 6). Tectonic restoration of ~360 km slip on the San Andreas fault aligns ca. 105–100 Ma basement of the northernmost Salinian block (i.e., MM—Montara Mountain) with the Recruit Pass deep-water fan system, but it creates a misalignment of Pinnacles and Neenach volcanic complexes, as well as San Juan Bautista (SJB) and San Emigdio Mountains (SEM) strata. Detrital zircon U-Pb age fractions are shown as pie diagrams corresponding to basement ages of the Cordilleran arc and Cenozoic volcanic rocks. Bold dashed line demarcates lower Th/U ratios of Cretaceous–Jurassic detrital zircon derived from the Sierra Nevada batholith from higher Th/U ratios derived from the Mojave block. Other geographic features: BL—Ben Lomond Mountain; GR—Gabilan Range; SNB—Sierra Nevada batholith.

ca. 23 Ma Pinnacles and Neenach volcanic complexes (Matthews, 1976).

Figure 13 shows the 45 km discrepancy between the newly proposed Montara Mountain–Recruit Pass correlation and the Pinnacles-Neenach volcanics. While these incongruent displacement estimates from coeval features seem to be in conflict, we consider this discrepancy to be revealing of the complexities of the plate boundary. In previous work, there has been a tendency in the study of the San Andreas and similar strike-slip faults to treat displaced crustal blocks as rigid objects that are translated to satisfy single or corresponding one-dimensional tie points through time (e.g., Matthews, 1976; Burnham, 2009). Specifically, most published palinspastic reconstructions of the northern San Andreas transform margin translate the Salinian block to the southeast without accounting for off-fault deformation on either side of the plate boundary. In other words, it is tempting to try to apply a single displacement history to the entire trace of the fault (e.g., competing models in Fig. 3). There are many features along the transform margin, outlined below, that have been recognized to have caused significant crustal deformation (e.g., extension of the La Honda basin and contraction of the southern San Joaquin basin; Stanley, 1985; Namson and Davis, 1988), such that the distances between piercing points on the same side of the fault (Fig. 13) would have changed over time; however, estimating the amount of deformation is often a challenge. We propose that the discrepancy between the Montara–Recruit Pass and Pinnacles-Neenach piercing points is the result of a net ~45 km of northwest-southeast–directed off-fault deformation that occurred on one or the other side of the fault since the early Miocene. This off-fault deformation consisted of either fault-parallel elongation on the northwest side of the San Andreas fault (between Montara Mountain and the Pinnacles volcanic center) or shortening on the southeast side of the fault (between Recruit Pass and the Neenach volcanic center), or a combination of the two.

A similar hypothesis of differential slip through off-fault deformation has been previously invoked for the post–16 Ma slip history of the San Gregorio–Hosgri fault, a subsidiary fault west of the San Andreas fault (Fig. 2). Colgan and Stanley (2016) proposed the effects of transrotation of the Transverse Ranges and shearing throughout the Santa Maria basin of the southern Salinian block to explain south-to-north, gradually increasing dextral offset along the San Gregorio–Hosgri fault. These displacements range from 0 km at the southern terminus with the clockwise-rotating western Transverse Ranges to greater than 150 km of displacement north of the zone of deformation. Furthermore, Darin and Dorsey (2013) proposed a similar model for explaining apparent slip discrepancies among three previously recognized cross-fault markers along the

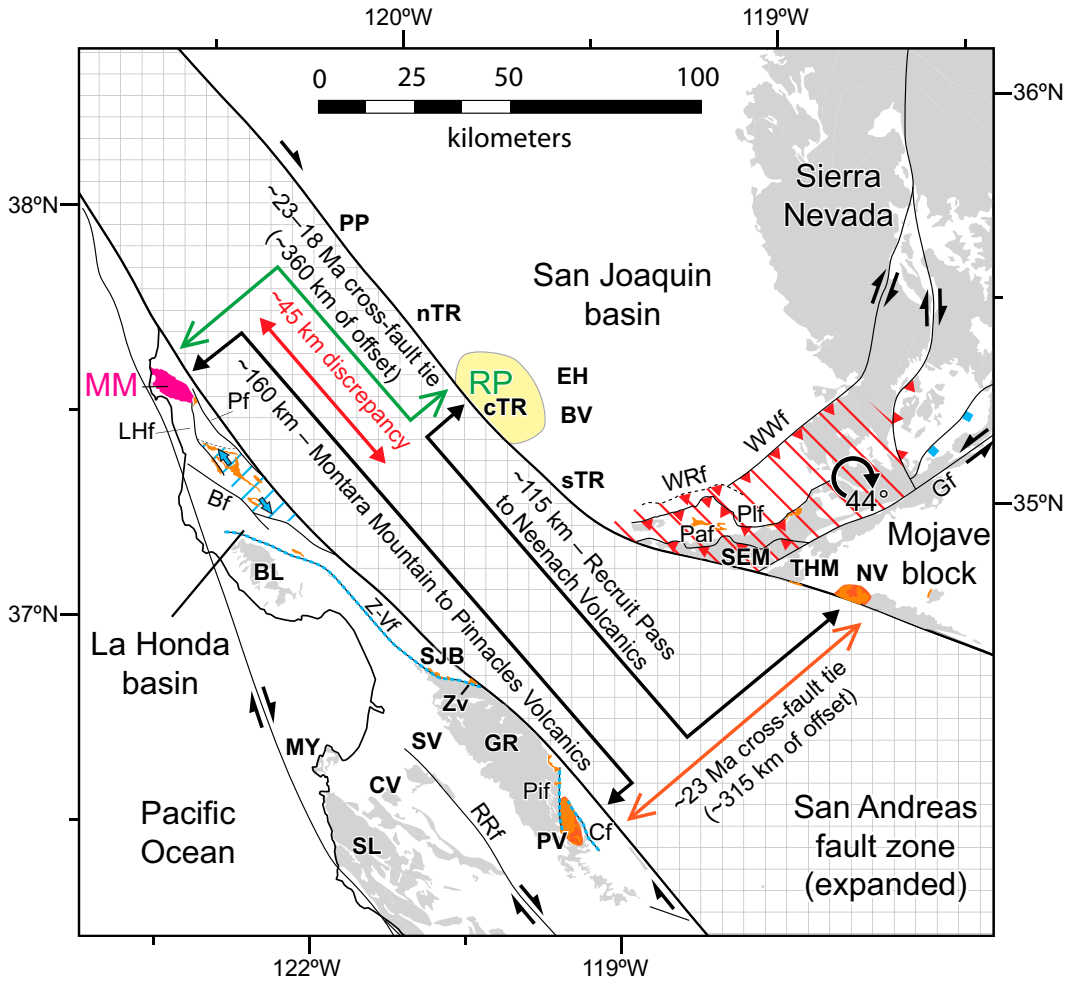

Figure 13. Map showing pre–16 Ma palinspastic alignment of Pinnacles and Neenach volcanic complexes (~315 km offset) with Mesozoic plutonic rocks (gray) and Cenozoic volcanic rocks (orange). Trace of the future San Andreas fault zone is expanded (cross-hatched area) to highlight cross-fault correlations and to annotate distances between key geologic features. Granitic basement of northernmost Salinian block (pink) is misaligned with Cenozoic deep-water fan (yellow) of the central Temblor Range (this study; ~360 km offset) by ~45 km. Faults and structural domains that have resulted in postdepositional northwest-southeast extension (blue) or shortening (red) of the Salinian block and Sierra Nevada block are shown. Note that longitude and latitude indicated west and east of the San Andreas fault are respective to modern locations of the Salinian block and North America. Faults: Bf—Butano fault; Cf—Chalone fault; Gf—Garlock fault; LHf—La Honda fault; Paf—Pastoria fault; Pf—Pilarcitos fault; Pif—Pinnacles fault; Plf—Pleito fault; RRf—Rinconada-Reliz fault; WRf—Wheeler Ridge fault; WWf—White Wolf fault; Z-Vf—Zayante-Vergeles fault. Geographic features of the Salinian block: BL—Ben Lomond Mountain; CV—Carmel Valley; GR—Gabilan Range; MM—Montara Mountain; MY—Monterey Peninsula; PV—Pinnacles Volcanics; SJB—San Juan Bautista; SL—Santa Lucia Range; SV—Salinas Valley; Zv—Zayante volcanics. Geographic features of the San Joaquin basin and Mojave Desert: BV—Buena Vista field; EH—Elk Hills field; NV—Neenach volcanics; PP—Polonio Pass; SEM—San Emigdio Mountains; THM—Tehachapi Mountains; TR—Temblor Range (n—north, c—central, s—south). Depositional tie: RP—Recruit Pass fan.

southern San Andreas fault, invoking extensional elongation during transrotation of the eastern Transverse Ranges as a plausible explanation.

The structural features along the San Andreas fault in central California that produced either northwest-southeast elongation across the Salinian block or shortening on the southern Sierra Nevada block are highlighted in Figure 13 and are summarized in Supplementary Table S6 (see footnote 1). We present two end-member solutions for reconciling the apparent ~45 km disparity in displacement between the offset of the Pinnacles and Neenach volcanics and the proposed offset of granitic basement of the northern Salinian block with the central Temblor Range (Fig. 14). These models are not mutually exclusive, and palinspastic reconstruction of the central California margin likely requires a combination of these end-member styles of off-fault deformation.

Model 1: Post–Early Miocene Transrotational Shear of the Tehachapi Block

Paleomagnetic studies of rocks in the San Emigdio Mountains and Tehachapi Range (Fig. 1) have demonstrated that the southern San Joaquin basin and "tail" of the Sierra Nevada batholith ("Tehachapi block" of Dickinson, 1996) have experienced up to 90° of clockwise rotation since Cretaceous time, 44° of which occurred between ca. 22 and 16 Ma (Kanter and McWilliams, 1982; Plescia and Calderone, 1986; Graham et al., 1990; Goodman and Malin, 1992). The rotation of the Tehachapi block significantly altered the geometry of the basin but has largely not been applied to paleogeographic reconstructions (for an exception, see Goodman and Malin, 1992).

In an attempt to reconcile an excess of >700 km Pacific–North America plate motion observed from seafloor magnetic anomalies (Stock and Molnar, 1988) relative to the estimated 315 km of slip on the San Andreas fault (Graham et al., 1989), Dickinson (1996) investigated the cumulative effects of transrotational shear (sensu Ingersoll, 1988) across the Transverse Ranges, Mojave, and Tehachapi blocks and displacement on subsidiary faults west of the San Andreas fault. Dickinson's (1996) study was monumental in demonstrating that global seafloor plate motions as implied by seafloor magnetic anomalies could be congruent across

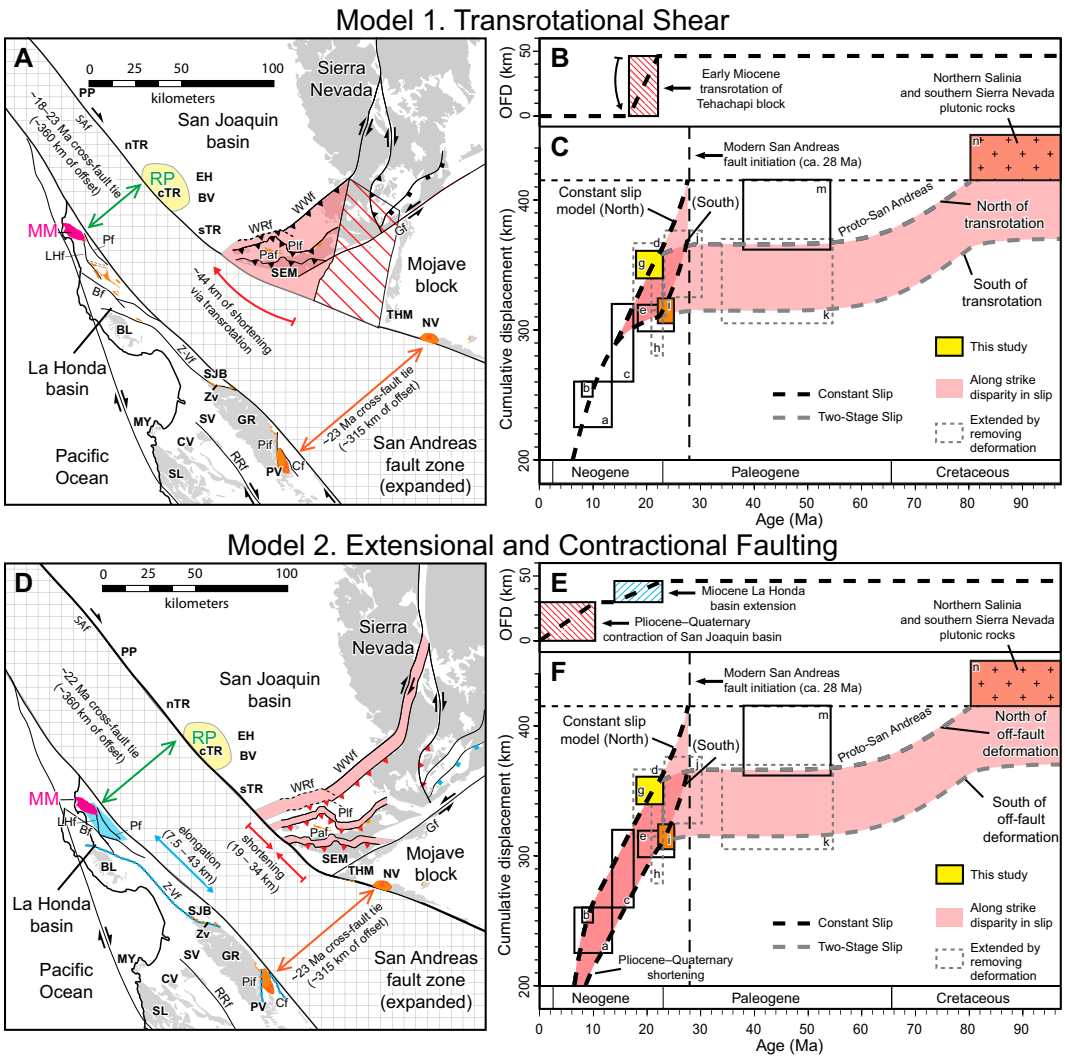

Figure 14. End-member models for reconciling the ~45 km disparity in displacement between the offset of the Pinnacles and Neenach volcanics (~315 km offset) and the proposed offset of granitic basement of the northern Salinian block with the central Temblor Range (~360 km offset). (A, D) Maps showing pre-Miocene (ca. 23 Ma) alignment of offset features with faults and structural domains of northwest-southeast extension (blue) and contraction (red), and restored areas highlighted (shaded blue or red). (B, E) Plots showing the off-fault deformation (OFD) caused by Salinian extension and Sierra Nevada–Mojave block shortening over time. (C, F) Plots displaying the resulting effect of OFD on the cumulative displacement history of the San Andreas fault (see Supplementary Table S2 [text footnote 1] for key cross-fault ties) north and south of the Tehachapi block. A two-stage slip model (gray dashed lines) includes initial displacement of Salinian granites along a proto–San Andreas fault, as opposed to a constant slip model (black dashed lines). In model 1 (A–C), early Miocene transrotational shear of the Tehachapi block (after Dickinson, 1996) accounts entirely for the disparity in San Andreas fault displacement, and displacement histories north and south of the Tehachapi block converge by ca. 16 Ma. In model 2 (D–F), OFD due to early Miocene Salinian extension and Pliocene–Quaternary contraction in the southern San Joaquin basin (see Supplementary Table S6 [text footnote 1] for estimates) results in presently converging slip histories. See Figure 13 for labels of faults, geographic features, and depositional ties.

continental tectonic boundaries, thereby resolving arguments against modern plate-tectonic theory (cf. Hill, 1971; Dickinson et al., 1972). Using 45° of clockwise rotation across the 60 km panel length of the Tehachapi block, Dickinson (1996) calculated that ~44 ± 8 km of margin-parallel shear occurred between 22 and 16 Ma (Fig. 14A). These relationships can be reconciled by dextral shearing of the western Mojave (i.e., northward translation of the Neenach volcanic center) and tectonic shortening of the southern San Joaquin basin (red shaded area in Fig. 14A). The estimated 44 km of margin-parallel shortening within the Tehachapi block that occurred during early Miocene time due to transrotation completely satisfies the approximate 45 km of slip disparity along the San Andreas fault proposed in this study.

Model 2: Post–Early Miocene Extension of the Salinian Block and Contraction of the Southern San Joaquin Basin

Significant extension of the La Honda pull-apart basin likely occurred during early to middle Miocene time. Considering that basin depth to extension relationships are typically 10%–20% in transtensional basins, Stanley (1985) estimated that northwest-southeast extension ranged from 7.5 to 35 km (15–25 km if only using the current extent of the Mindego Basalt). Stanley (1985) suspected that the La Honda pull-apart basin was a direct result of slip along the San Andreas fault, although other authors have ascribed the extension to the northward migration of the Mendocino fracture zone (e.g., Graham et al., 1989). Additionally, dextral transtension is believed to have occurred from ca. 14 to 6 Ma in a block between the San Andreas fault and Pinnacles volcanics (Graymer et al., 2013) and may have resulted in up to 8 km of fault-parallel elongation (Fig. 13).

Within the northern Salinian block, series of northwest-striking, high-angle faults (i.e., Butano, La Honda, Ben Lomond, and Zayante-Vergeles faults; Fig. 14D) were active during Oligocene through Miocene time and controlled patterns of sediment and volcanic deposition (Cummings et al., 1962; Clark and Rietman, 1973; Stanley and McCaffrey, 1983); however, the timing and amount of strike-slip displacement along these faults, if any, are uncertain (Stanley, 1985). Furthermore, fold axes throughout the La Honda basin also strike northwest and increase in abundance northward and with proximity to

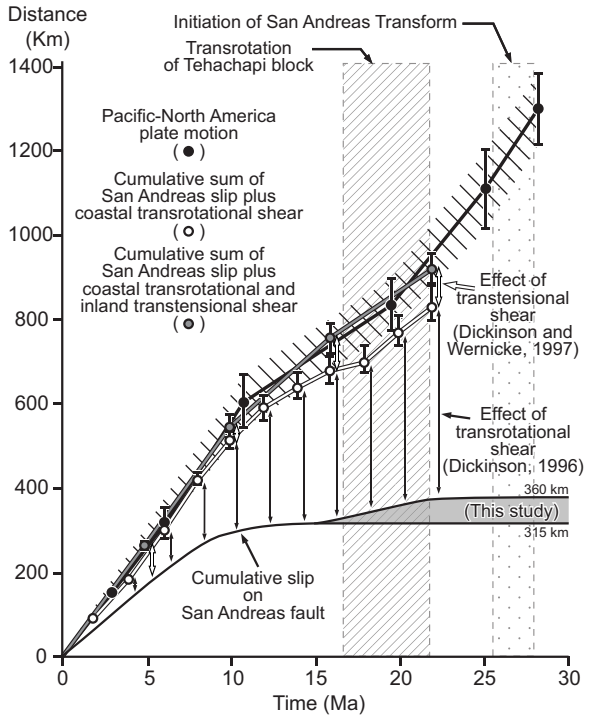

Figure 15. Comparison of cumulative displacement of the central California transform margin, as inferred from (1) relative rotation of the Pacific–North American plates, and (2) cumulative slip of the San Andreas fault and incremental effects of shear from coastal transrotational domains across the central California margin (modified from Dickinson, 1996) and inland extension across the Basin and Range (Dickinson and Wernicke, 1997). The newly proposed amount of 360 km of slip on the San Andreas fault (this study) north of the transrotational domains reconciles the previously reported discrepancy in early Miocene displacement. Refer to table 4 of Dickinson (1996) and table 1 of Dickinson and Wernicke (1997) for calculation of the cumulative effects of transrotational and transtensional domains on the San Andreas transform margin.

the San Andreas fault. Although the structural folding occurred across the basin, deformation is only slightly oblique to the San Andreas fault (Fig. 4) and would have had only minimal effect on fault-parallel shortening of the Salinian block.

In comparison, contractional features within the southern San Joaquin basin and San Emigdio Mountains include several northward-verging reverse faults that have been active since the Pliocene (Fig. 14D; Davis, 1983; Davis, 1986; Dibblee, 1986; Namson and Davis, 1988; Wood and Saleeby, 1997). These faults (e.g., White Wolf, Wheeler Ridge, Pleito, and Pastoria faults) have been extensively mapped with varying estimates of shortening. For example, Namson and Davis estimated >19 km of shortening across the Pleito, Pastoria, and associated blind thrusts north of the San Andreas fault, while restoration of the schematic cross section of Niemi et al. (2013) produced 12–15 km of shortening. The Wheeler Ridge and White Wolf faults are located on the northern end of this zone of deformation (Fig. 14D), and the latter is estimated to have had up to 15 km of northwest-southeast shortening and significant right-lateral strike-slip displacement (Chapman et al., 2010).

The net effects of faulting adjacent to the San Andreas fault (off-fault deformation) that resulted in the Cenozoic northwest-southeast elongation of the Salinian block (between the Pinnacles and Montara Mountain) and the shortening of the southern San Joaquin basin (between the Neenach volcanics and central Temblor Range) are more than sufficient to account for the 45 km of apparent slip discrepancy along the San Andreas fault (Fig. 14D; see Supplementary Table S6 for a complete list of features).

Implications for San Andreas Fault Slip History and Relative Pacific–North American Plate Motion

The timing of the off-fault deformation from transrotational shear (model 1) or Salinian extension and San Joaquin basin shortening (model 2) is summarized in Figures 14B and 14E. The resulting effect of each of these models on plate deformation is a disparity in the slip histories of the San Andreas fault south (i.e., Pinnacles-Neenach correlation) and north of the Tehachapi block (i.e., Montara–Recruit Pass correlation), as shown in Figures 14C and 14F. In the transrotational model 1, slip histories converge by the end of early Miocene time (ca. 16 Ma), while in model 2, with extensional and contractional faulting, slip histories are presently converging.

Regardless of the model of off-fault deformation, a major implication of both models is that pre–28 Ma displacement on the San Andreas is not required. While Sharman et al. (2013) required 50–75 km of post-Eocene to late Oligocene displacement (Fig. 3), this study's additional Oligocene–Lower Miocene constraint on the correlation of the northern Salinian block and western San Joaquin basin effectively removed the minimum pre-Oligocene displacement estimate of their Eocene cross-fault tie (i.e., Mojave Desert provenance of the Butano Sandstone; point "m" on Figs. 14C and 14E) while retaining previous correlations that were in apparent conflict (Eocene forearc strata of northern Gabilan Range and San Emigdio Mountains; point "k"; also see Fig. 3). With the present information available, we cannot resolve whether the displacement of the Salinian block occurred entirely on the San Andreas fault (constant slip model) or whether a portion of this displacement also occurred on a predecessor fault (two-stage model; e.g., Suppe, 1970), so we chose to show both scenarios in Figures 14C and 14F. In the scenario of constant slip, the Salinian block would have been displaced continuously by ~415 km since the initiation of the San Andreas fault (ca. 28 Ma), with ~55 km of displacement prior to deposition of the Recruit Pass Sandstone during the early Miocene (Figs. 14C and 14F). Conversely, the two-stage slip model allows up to 55 km of initial right-lateral displacement of the Late Cretaceous Salinian basement prior to Eocene time (ca. 56 Ma), followed by 360 km of San Andreas fault displacement.

Finally, the sum of transrotational shear across multiple structural domains and cumulative slip on the San Andreas fault was shown by Dickinson (1996) to satisfy most of the relative Pacific–North American plate slip budget, although a slip deficit of ~100 km remained unaccounted for in that study. Dickinson and Wernicke (1997) further considered additional effects of Cenozoic WNW-directed extension of the Basin and Range Province. This adjustment satisfactorily resolved post–16 Ma relative plate motions but continued to result in an apparent early Miocene discrepancy in displacement. The authors hypothesized that this might be due to deformational events associated with the capture of the Monterey microplate during the development of the transform margin. However, by using the apparent slip history of the Pinnacles-Neenach offset for the San Andreas fault (Fig. 3; Matthews, 1976; Graham et al., 1989), the >45 km deficit in right-lateral slip demonstrated in this study effectively cancels out the shear that Dickinson (1996) attributed to the Tehachapi block to the north. Instead, it is imperative that the total slip history for the San Andreas fault north of all shear domains is used in order to rectify discrepancies with the relative plate motion budget. When our revised San Andreas fault slip history of 360 km of offset since the early Miocene time (Fig. 14) is applied with

Dickinson's (1996) estimates of transrotational shear for all domains to the south and Dickinson and Wernicke's (1997) extension of the Basin and Range, this discrepancy is reconciled (Fig. 15). This resolution of relative plate motion with cumulative dextral shear along the western North American continental plate boundary not only supports our new cross-fault correlation and slip magnitude of the San Andreas fault, but it also presents a solution for a tectonic puzzle that has been under investigation for nearly five decades (Hill, 1971; Dickinson et al., 1972; Dickinson and Wernicke, 1997).

CONCLUSIONS

Despite similar petrographic composition, new detrital zircon data from the Castle Rock and Recruit Pass submarine fans of the Vaqueros and Temblor Formations suggest a dissimilar provenance, which challenges their established correlation and use as a cross-fault marker to estimate San Andreas fault offset. Instead, the Oligocene–Miocene sandstones of the northern Salinian block have similar detrital zircon age distributions as, and probable recycling from, the underlying Eocene Butano Sandstone that was derived from the southern Sierra Nevada and western Mojave Desert. Strata of the western San Joaquin basin have a spatially diverse provenance history. Specifically, sandstones in the central Temblor Range (e.g., Recruit Pass fan) were derived from the granitic basement of the northernmost Salinian block, while southern San Joaquin basin sandstones are more similar to those of the La Honda basin. These spatial relationships are best resolved by restoring 360 km or more of displacement on the San Andreas fault since early Miocene time. Disparity in this slip magnitude with the coeval 315 km of slip on the Pinnacles and Neenach volcanic centers is due to at least 45 km of off-fault deformation along the central California transform margin. This new constraint removes the need for, but does not preclude, controversial Paleogene slip on the San Andreas or precursor faults and solves an early Miocene slip deficit between Pacific–North American relative plate motion and displacement across the transform margin.

ACKNOWLEDGMENTS

We thank Ziva Shulaker and Nora Nieminski for providing field assistance. Trevor Dumitru and Katie Dunn helped with mineral separation at the Stanford Earth Materials Laboratory, and we thank Arizona LaserChron Center, which is funded in part by the National Science Foundation (NSF) Instrumentation and Facilities Division. This work benefited from discussions with Marty Grove, Curtis Baden, George Hilley, Zach Sickmann, Carl Jacobsen, and Ray Ingersoll. Constructive reviews by Mike Darin and an anonymous reviewer greatly improved the quality and clarity of this manuscript. Funding for this research was provided by the industrial affiliates of the Stanford Project on Deep-water Depositional Systems (SPODDS). We thank Occidental Petroleum for providing core samples from the San Joaquin basin. We are grateful for the students of the "Stanford Petroleum Geology Industrial Affiliates Program" (1982–1999) for archiving rock samples from the San Joaquin basin that were used for several analyses.

REFERENCES CITED

Andersen, T., Kristoffersen, M., and Elburg, M.A., 2018, Visualizing, interpreting and comparing detrital zircon age and Hf isotope data in basin analysis—A graphical approach: Basin Research, v. 30, p. 132–147, https://doi.org/10.1111/bre.12245.

Armijo, R., Meyer, B., Hubert, A., and Barka, A., 1999, Westward propagation of the North Anatolian fault into the northern Aegean: Timing and kinematics: Geology, v. 27, no. 3, p. 267–270, https://doi.org/10.1130/0091-7613(1999)027<0267:WPOTNA>2.3.CO;2.

Atwater, T., 1970, Implications of plate tectonics for the Cenozoic tectonic evolution of western North America: Geological Society of America Bulletin, v. 81, p. 3513–3536, https://doi.org/10.1130/0016-7606(1970)81[3513:IOPTFT]2.0.CO;2.

Atwater, T., 1989, Plate tectonic history of the northeast Pacific and western North America, *in* Winterer, E.L., et al., eds., The Eastern Pacific Ocean and Hawaii: Boulder, Colorado, Geological Society of America, Geology of North America, v. N, p. 21–72.

Atwater, T., and Molnar, P., 1973, Relative motion of the Pacific and North American plates deduced from seafloor spreading in the Atlantic, Indian, and South Pacific Oceans, *in* Kovach, R.L., and Nur, A., eds., Proceedings of the Conference on Tectonic Problems of the San Andreas Fault System: Stanford University Publications in Geological Science, v. 12, p. 136–148.

Bandy, O.L., and Arnal, R.E., 1969, Middle Tertiary basin development, San Joaquin Valley, California: Geological Society of America Bulletin, v. 80, p. 783–820, https://doi.org/10.1130/0016-7606(1969)80[783:MTBDSJ]2.0.CO;2.

Bartow, J.A., 1991, The Cenozoic Evolution of the San Joaquin Valley, California: U.S. Geological Survey Professional Paper 1501, 40 p., https://doi.org/10.3133/pp1501.

Bartow, J.A., 1992, Cenozoic stratigraphy of the northern San Joaquin Valley, central California, *in* Erskin, M.E., Unruh, J., Lettis, W.R., and Bartow, J.A., eds., Field Guide to the Tectonics of the Boundary Between the California Central Coast Ranges and the Great Valley of California: Bakersfield, California, American Association of Petroleum Geologists, Pacific Section, p. 5–12.

Bent, J.V., 1985, Provenance of Upper Oligocene–Middle Miocene sandstones of the San Joaquin basin, California, *in* Graham, S.A., ed., Geology of the Temblor Formation, Western San Joaquin Basin, California: Los Angeles, California, Society of Economic Paleontologists and Mineralogists, Pacific Section, p. 97–120.

Bloch, R.B., Von Huene, R., Hart, P., and Wentworth, C.M., 1993, Style and magnitude of tectonic shortening normal to the San Andreas fault across Pyramid Hills and Kettleman Hills Dome, California: Geological Society of America Bulletin, v. 105, p. 464–478, https://doi.org/10.1130/0016-7606(1993)105<0464:SAMOTS>2.3.CO;2.

Bouchet, R.A., Blichert-Toft, J., Reid, M.R., Levander, A., and Albarède, F., 2014, Similarities between the Th/U map of the western US crystalline basement and the seismic properties of the underlying lithosphere: Earth and Planetary Science Letters, v. 391, p. 243–254, https://doi.org/10.1016/j.epsl.2014.02.004.

Breiter, K., 2016, Monazite and zircon as major carriers of Th, U, and Y in peraluminous granites: Examples from the Bohemian Massif: Mineralogy and Petrology, v. 110, no. 6, p. 767–785, https://doi.org/10.1007/s00710-016-0448-0.

Burnham, K., 2009, Predictive model of San Andreas fault system paleogeography, Late Cretaceous to early Miocene, derived from detailed multidisciplinary conglomerate correlations: Tectonophysics, v. 464, p. 195–258, https://doi.org/10.1016/j.tecto.2007.11.056.

Carter, J.B., 1985, Depositional environments of the type Temblor Formation, Chico Martinez Creek, Kern County, California, *in* Graham, S.A., ed., Geology of the Temblor Formation, Western San Joaquin Basin, California: Society of Economic Paleontologists and Mineralogists, Pacific Section, Book 44, p. 5–18.

Champion, D.E., 1989, Identification of the Rinconada fault in western San Mateo County, CA through the use of strontium isotopic studies: Geological Society of America Abstracts with Programs, v. 21, no. 5, p. 64.

Champion, D.E., and Kistler, R.W., 1991, Paleogeographic reconstruction of northern Salinia using Sr isotopic properties: Geological Society of America Abstracts with Programs, v. 23, no. 2, p. 12.

Chapman, A.D., Kidder, S., Saleeby, J.B., and Ducea, M.N., 2010, Role of extrusion of the Rand and Sierra de Salinas schists in Late Cretaceous extension and rotation of the southern Sierra Nevada and vicinity: Tectonics, v. 29, no. 5, p. 1–21, https://doi.org/10.1029/2009TC002597.

Clarke, S.H., Jr., 1973, The Eocene Point of Rocks Sandstone-Provenance, mode of deposition, and implications for the history of offset along the San Andreas fault in central California [Ph.D. thesis]: Berkeley, University of California, 302 p.

Clarke, S.H., Jr., and Nilsen, T.H., 1973, Displacement of Eocene strata and implications for the history of offset along the San Andreas fault, central and northern California, *in* Kovach, R.L., and Nur, A., eds., Proceedings of the conference on tectonic problems of the San Andreas fault system: Stanford University Publications in Geological Sciences, v. 13, p. 358–367.

Clark, J.C., and Rietman, J.D., 1973, Oligocene Stratigraphy, Tectonics, and Paleogeography Southwest of the San Andreas Fault, Santa Cruz Mountains and Gabilan Range, California Coast Ranges: U.S. Geological Survey Professional Paper 783, 18 p., https://doi.org/10.3133/pp783.

Colgan, J.P., and Stanley, R.G., 2016, The Point Sal–Point Piedras Blancas correlation and the problem of slip on the San Gregorio–Hosgri fault, central California Coast Ranges: Geosphere, v. 12, p. 971–984, https://doi.org/10.1130/GES01289.1.

Coutts, D.S., Matthews, W.A., and Hubbard, S.M., 2019, Assessment of widely used methods to derive depositional ages from detrital zircon populations: Geoscience Frontiers, v. 10, p. 1421–1435, https://doi.org/10.1016/j.gsf.2018.11.002.

Cummings, J.C., Touring, R.M., and Brabb, E.E., 1962, Geology of the northern Santa Cruz Mountains, California, *in* Bowen, O.E., Jr., ed., Geologic Guide to the Gas and Oil Fields of Northern California: California Division of Mines and Geology Bulletin 181, p. 179–220.

Darin, M.H., and Dorsey, R.J., 2013, Reconciling disparate estimates of total offset on the southern San Andreas fault: Geology, v. 41, no. 9, p. 975–978, https://doi.org/10.1130/G34276.1.

Davis, T.L., 1983, Late Cenozoic Structure and Tectonic History of the Western "Big Bend" of the San Andreas Fault and Adjacent San Emigdio Mountains [Ph.D. thesis]: Santa Barbara, California, University of California–Santa Barbara, 578 p., 4 plates.

Davis, T.L., 1986, A structural outline of the San Emigdio Mountains, *in* Davis, T.L., and Namson, J., eds., Geologic Transect Across the Western Transverse Ranges: Bakersfield, California, Society of Economic Paleontologists and Mineralogists, Pacific Section, Guidebook, p. 23–32.

Dibblee, T.W., Jr., 1973, Stratigraphy of the Southern Coast Ranges near the San Andreas Fault from Cholame to Maricopa, California: U.S. Geological Survey Professional Paper 764, 45 p., https://doi.org/10.3133/pp764.

Dibblee, T.W., Jr., 1986, Geology of the San Emigdio Mountains, California, Field Trip Guidebook: Society of Economic Paleontologists and Mineralogists, Pacific Section, Book 48, p. 1–10.

Dickinson, W.R., 1996, Kinematics of Transrotational Tectonism in the California Transverse Ranges and its Contribution to Cumulative Slip along the San Andreas

Transform Fault System: Geological Society of America Special Paper 305, 46 p., https://doi.org/10.1130/0-8137-2305-1.

Dickinson, W.R., 2008, Impact of differential zircon fertility of granitoid basement rocks in North America on age populations of detrital zircons and implications for granite petrogenesis: Earth and Planetary Science Letters, v. 275, p. 80–92, https://doi.org/10.1016/j.epsl.2008.08.003.

Dickinson, W.R., and Gehrels, G.E., 2009, Use of U-Pb ages of detrital zircons to infer maximum depositional ages of strata: A test against a Colorado Plateau Mesozoic database: Earth and Planetary Science Letters, v. 288, p. 115–125, https://doi.org/10.1016/j.epsl.2009.09.013.

Dickinson, W.R., and Wernicke, B.P., 1997, Reconciliation of San Andreas slip discrepancy by a combination of interior Basin and Range extension and transrotation near the coast: Geology, v. 25, p. 663–665, https://doi.org/10.1130/0091-7613(1997)025<0663:ROSASD>2.3.CO;2.

Dickinson, W.R., Cowan, D.S., and Schweickert, R.A., 1972, Test of the new global tectonics [Discussion]: American Association of Petroleum Geologists Bulletin, v. 56, p. 375–384.

Dickinson, W.R., Ducea, M., Rosenberg, L.I., Greene, H.G., Graham, S.A., Clark, J.C., Weber, G.E., Kidder, S., Ernst, W.G., and Brabb, E.E., 2005, Net Dextral Slip, Neogene San Gregorio–Hosgri Fault Zone, Coastal California: Geologic Evidence and Tectonic Implications: Geological Society of America Special Paper 391, 43 p., https://doi.org/10.1130/0-8137-2391-4.

Dumitru, T.A., Ernst, W.G., Hourigan, J.K., and McLaughlin, R.J., 2015, Detrital zircon U-Pb reconnaissance of the Franciscan subduction complex in northwestern California: International Geology Review, v. 57, p. 767–800, https://doi.org/10.1080/00206814.2015.1008060.

Gehrels, G.E., Valencia, V.A., and Ruiz, J., 2008, Enhanced precision, accuracy, efficiency, and spatial resolution of U-Pb ages by laser ablation–multicollector–inductively coupled plasma–mass spectrometry: Geochemistry Geophysics Geosystems, v. 9, Q03017, https://doi.org/10.1029/2007GC001805.

Gillespie, B.W., 1986, The Temblor Formation: Maricopa to the Eastern San Emigdio Mountains, Kern County, California [M.S. thesis]: Stanford, California, Stanford University, 161 p.

Goodman, E.D., and Malin, P.E., 1992, Evolution of the southern San Joaquin basin and mid- Tertiary "transitional" tectonics, central California: Tectonics, v. 11, no. 3, p. 478–498, https://doi.org/10.1029/91TC02871.

Gooley, J.T., Grove, M., and Graham, S.A., 2020, Tectonic evolution of the central California margin as reflected by detrital zircon composition in the Mount Diablo region, *in* Sullivan, R., Sloan, D., and Unruh, J.R., eds., Geological Framework of Mount Diablo: Geological Society of America Memoir (in press).

Gordon, G., Fisher, E., Myers, G., and Boles, J., 2017, Paleogeographic controls on reservoir quality in the Carneros turbidite systems, San Joaquin Basin, California, *in* American Association of Petroleum Geologists 2017 Pacific Section Annual Meeting: American Association of Petroleum Geologists Search and Discovery article 90302.

Graham, S.A., 1978, Role of Salinian block in evolution of San Andreas fault system, California: American Association of Petroleum Geologists Bulletin, v. 62, p. 2214–2231.

Graham, S.A., McCloy, C., Hitzman, M., Ward, R., and Turner, R., 1984, Basin evolution during change from convergence to transform continental margin in central California: American Association of Petroleum Geologists Bulletin, v. 68, p. 233–349.

Graham, S.A., Stanley, R.G., Bent, J.V., and Carter, J.B., 1989, Oligocene and Miocene paleogeography of central California and displacement along the San Andreas fault: Geological Society of America Bulletin, v. 101, p. 711–730, https://doi.org/10.1130/0016-7606(1989)101<0711:OAMPOC>2.3.CO;2.

Graham, S.A., DeCelles, P.G., Carroll, A.R., and Goodman, E.D., 1990, Middle Tertiary contractile deformation, uplift, extension, and rotation in the San Emigdio Range, southern California: American Association of Petroleum Geologists Search and Discovery article 91003.

Graymer, R.W., Stanley, R.G., Roberts, M.A., Barron, J.A., and McPhee, D.K., 2013, Geologic mapping, gravity, and paleontological studies in the Pinnacles National Park region, central California, reveal ~14 to ~6 Ma transtensional history of the San Andreas fault system: Geological Society of America Abstracts with Programs, v. 45, no. 6, p. 58.

Henry, C.D., and Faulds, J.E., 2010, Ash-flow tuffs in the Nine Hill, Nevada, paleovalley and implications for tectonism and volcanism of the western Great Basin, USA: Geosphere, v. 6, p. 339–369, https://doi.org/10.1130/GES00548.1.

Henry, C.D., Hinz, N.H., Faulds, J.E., Colgan, J.P., John, D.A., Brooks, E.R., Cassel, E.J., Garside, L.J., Davis, D.A., and Castor, S.B., 2012, Eocene–early Miocene paleotopography of the Sierra Nevada–Great Basin–Nevadaplano based on widespread ash-flow tuffs and paleovalleys: Geosphere, v. 8, p. 1–27, https://doi.org/10.1130/GES00727.1.

Herriott, T.M., Crowley, J.L., Schmitz, M.D., Wartes, M.A., and Gillis, R.J., 2019, Exploring the law of detrital zircon: LA-ICP-MS and CA-TIMS geochronology of Jurassic forearc strata, Cook Inlet, Alaska, USA: Geology, v. 47, p. 1044–1048, https://doi.org/10.1130/G46312.1.

Hill, M.L., 1971, A test of new global tectonics: Comparisons of northeast Pacific and California structures: The American Association of Petroleum Geologists Bulletin, v. 55, p. 3–9.

Huffman, O.F., 1972, Lateral displacement of Upper Miocene rocks and the Neogene history of offset along the San Andreas fault in central California: Geological Society of America Bulletin, v. 83, p. 2913–2946, https://doi.org/10.1130/0016-7606(1972)83[2913:LDOUMR]2.0.CO;2.

Ingersoll, R.V., 1988, Tectonics of sedimentary basins: Geological Society of America Bulletin, v. 100, p. 1704–1719, https://doi.org/10.1130/0016-7606(1988)100<1704:TOSB>2.3.CO;2.

Jacobson, C.E., Grove, M., Pedrick, J.N., Barth, A.P., Marsaglia, K.M., Gehrels, G.E., and Nourse, J.A., 2011, Late Cretaceous–early Cenozoic tectonic evolution of the southern California margin inferred from provenance of trench and forearc sediments: Geological Society of America Bulletin, v. 123, p. 485–506, https://doi.org/10.1130/B30238.1.

Jennings, C.W., Strand, R.G., and Rogers, T.H., 1977, Geologic Map of California: Sacramento, California, California Division of Mines and Geology, scale 1:750,000.

Johnson, C.L., and Graham, S.A., 2007, Middle Tertiary stratigraphic sequences of the San Joaquin basin, California, *in* Scheirer, A.H., ed., Petroleum Systems and Geologic Assessment of Oil and Gas in the San Joaquin Basin Province, California: U.S. Geological Survey Professional Paper 1713, p. 1–18.

Kanter, L.R., and McWilliams, M.O., 1982, Rotation of the southernmost Sierra Nevada: Journal of Geophysical Research, v. 87, p. 3819–3830, https://doi.org/10.1029/JB087iB05p03819.

King, P.R., 2000, Tectonic reconstructions of New Zealand: 40 Ma to the present: New Zealand Journal of Geology and Geophysics, v. 43, p. 611–638, https://doi.org/10.1080/00288306.2000.9514913.

Kistler, R.W., and Champion, D.E., 2001, Rb-Sr Whole-Rock and Mineral Ages, K-Ar, 40Ar/39Ar, and U-Pb Mineral Ages, and Strontium, Lead, Neodymium, and Oxygen Isotopic Compositions for Granitic Rocks from the Salinian Composite Terrane, California: U.S. Geological Survey Open-File Report 01-453, 84 p., https://doi.org/10.3133/ofr01453.

Lamb, S., Mortimer, N., Smith, E., and Turner, G., 2016, Focusing of relative plate motion at a continental transform fault: Cenozoic dextral displacement >700 km on New Zealand's Alpine fault, reversing >225 km of Late Cretaceous sinistral motion: Geochemistry Geophysics Geosystems, v. 17, p. 1197–1213, https://doi.org/10.1002/2015GC006225.

Lechler, A.R., and Niemi, N.A., 2011, Sedimentologic and isotopic constraints on the Paleogene paleogeography and paleotopography of the southern Sierra Nevada, California: Geology, v. 39, p. 379–382, https://doi.org/10.1130/G31535.1.

Malkowski, M.A., Sharman, G.R., Johnstone, S., Grove, M.J., Kimbrough, D.L., and Graham, S.A., 2019, Dilution and propagation of provenance trends in sand and mud: Geochemistry and detrital zircon geochronology of modern sediment from central California (U.S.A.): American Journal of Science, v. 319, p. 846–902, https://doi.org/10.2475/10.2019.02.

Matthews, V., III, 1973, Pinnacles-Neenach correlation: A restriction for models of the origin of the Transverse Ranges and the Big Bend in the San Andreas fault: Geological Society of America Bulletin, v. 84, p. 683–688, https://doi.org/10.1130/0016-7606(1973)84<683:PCARFM>2.0.CO;2.

Matthews, V., III, 1976, Correlation of Pinnacles and Neenach volcanic fields and their bearing on San Andreas fault problem: American Association of Petroleum Geologists Bulletin, v. 60, p. 2128–2141.

Mattinson, J.M., 1994, A study of complex discordance in zircons using step-wise dissolution techniques: Contributions to Mineralogy and Petrology, v. 116, p. 117–129, https://doi.org/10.1007/BF00310694.

McDougall, K., 2008, California Cenozoic biostratigraphy—Paleogene (chapter 4), *in* Scheirer, A.H., ed., Petroleum Systems and Geologic Assessment of Oil and Gas in the San Joaquin Basin Province, California: U.S. Geological Survey Professional Paper 1713, 30 p.

McKay, M.P., Jackson, W.T., Jr., and Hessler, A.M., 2018, Tectonic stress regime recorded by zircon Th/U: Gondwana Research, v. 57, p. 1–9, https://doi.org/10.1016/j.gr.2018.01.004.

McWilliams, M.O., and Li, Y., 1985, Oroclinal rotation of the southern Sierra Nevada batholith: Science, v. 230, p. 172–175, https://doi.org/10.1126/science.230.4722.172.

Mortimer, N., 2014, The oroclinal bend in the South Island, New Zealand: Journal of Structural Geology, v. 64, p. 32–38, https://doi.org/10.1016/j.jsg.2013.08.011.

Mortimer, N., 2018, Evidence for a pre-Eocene proto–Alpine fault through Zealandia: New Zealand Journal of Geology and Geophysics, v. 61, no. 3, p. 251–259, https://doi.org/10.1080/00288306.2018.1434211.

Namson, J.S., and Davis, T.L., 1988, Seismically active fold and thrust belt in the San Joaquin Valley, central California: Geological Society of America Bulletin, v. 100, p. 257–273, https://doi.org/10.1130/0016-7606(1988)100<0257:SAFATB>2.3.CO;2.

Niemi, N.A., 2013, Detrital zircon age distributions as a discriminator of tectonic versus fluvial transport: An example from the Death Valley, USA, extended terrane: Geosphere, v. 9, no. 1, p. 126–137, https://doi.org/10.1130/GES00820.1.

Niemi, N.A., Buscher, J.T., Spotila, J.A., House, M.A., and Kelley, S.A., 2013, Insights from low-temperature thermochronometry into transpressional deformation and crustal exhumation along the San Andreas fault in the western Transverse Ranges, California: Tectonics, v. 32, p. 1602–1622, https://doi.org/10.1002/2013TC003377.

Nilsen, T.H., 1984, Offset along the San Andreas fault of Eocene strata from the San Juan Bautista area and western San Emigdio Mountains, California: Geological Society of America Bulletin, v. 95, p. 599–609, https://doi.org/10.1130/0016-7606(1984)95<599:OATSAF>2.0.CO;2.

Nilsen, T.H., and Simoni, T.R., 1973, Deep-sea fan paleocurrent patterns of the Eocene Butano Sandstone, Santa Cruz Mountains, California: Journal of Research of the U.S. Geological Survey, v. 1, p. 439–452.

Page, B.M., 1981, The southern Coast Ranges, *in* Ernst, W.G., ed., The Geotectonic Development of California: Englewood Cliffs, New Jersey, Prentice-Hall, p. 329–417.

Pence, J.J., 1985, Sedimentology of the Temblor Formation in the northern Temblor Range, California, *in* Graham, S.A., ed., Geology of the Temblor Formation, Western San Joaquin Basin, California: Society of Economic Paleontologists and Mineralogists, Pacific Section, Book 44, p. 19–34.

Plescia, J.B., and Calderone, G.J., 1986, Paleomagnetic constraints on the timing and extent of rotation of the Tehachapi Mountains, California: Geological

Society of America Abstracts with Programs, v. 18, no. 2, p. 171.

Powell, R.E., 1993, Balanced palinspastic reconstruction of pre–late Cenozoic paleogeology, southern California: Geologic and kinematic constraints on evolution of the San Andreas fault system, *in* Powell, R.E., et al., eds., The San Andreas Fault System: Displacement, Palinspastic Reconstruction, and Geologic Evolution: Geological Society of America Memoir 178, p. 1–106, https://doi.org/10.1130/MEM178-p1.

Reid, S.A., 1995, Miocene and Pliocene depositional systems of the southern San Joaquin basin and formation of sandstone reservoirs in the Elk Hills area, California, *in* Fritsche, A.E., ed., Cenozoic Paleogeography of the Western United States–II: Pacific Section, Society for Sedimentary Geology (SEPM), Book 75, p. 131–150.

Riggs, N.R., Reynolds, S.J., Linder, P.J., Howell, E.R., Barth, A.P., Parker, W.G., and Walker, J.D., 2013, The early Mesozoic Cordilleran arc and Late Triassic paleotopography: The detrital record in Upper Triassic sedimentary successions on and off the Colorado Plateau: Geosphere, v. 9, p. 602–613, https://doi.org/10.1130/GES00860.1.

Riggs, N.R., Sanchez, T.B., and Reynolds, S.J., 2020, Evolution of the early Mesozoic Cordilleran arc: The detrital zircon record of back-arc basin deposits, Triassic Buckskin Formation, western Arizona and southeastern California, USA: Geosphere, v. 16, p. 1753–1768, https://doi.org/10.1130/GES02193.1.

Ritts, B.D., Yue, Y., and Graham, S.A., 2004, Oligocene–Miocene tectonics and sedimentation along the Altyn Tagh fault, northern Tibetan Plateau: Analysis of the Xorkol, Subei, and Aksay Basins: The Journal of Geology, v. 112, no. 2, p. 207–229, https://doi.org/10.1086/381658.

Ryder, R.T., and Thomson, A., 1989, Tectonically Controlled Fan Delta and Submarine Fan Sedimentation of Late Miocene Age, Southern Temblor Range, California: U.S. Geological Survey Professional Paper 1442, 59 p., https://doi.org/10.3133/pp1442.

Saylor, J.E., and Sundell, K.E., 2016, Quantifying comparison of large detrital geochronology data sets: Geosphere, v. 12, p. 203–220, https://doi.org/10.1130/GES01237.1.

Saleeby, J., Saleeby, Z., Robbins, J., and Gillespie, J., 2016, Sediment provenance and dispersal of Neogene–Quaternary strata of the southeastern San Joaquin basin and its transition into the southern Sierra Nevada, California: Geosphere, v. 12, p. 1744–1773, https://doi.org/10.1130/GES01359.1.

Seiders, V.M., and Cox, B.T., 1992, Place of Origin of the Salinian Block, California, as Based on Clast Compositions of Upper Cretaceous and Lower Tertiary Conglomerates: U.S. Geological Survey Professional Paper 1526, 80 p., https://doi.org/10.3133/pp1526.

Şengör, A.M.C., Tuysuz, O., Imren, C., Sakinc, M., Eyidogan, H., Gorur, N., Pchon, X.L., and Rangin, C., 2005, The North Anatolian fault: A new look: Annual Review of Earth and Planetary Sciences, v. 33, p. 37–112, https://doi.org/10.1146/annurev.earth.32.101802.120415.

Sharman, G.R., and Malkowski, M.A., 2020, Needles in a haystack: Detrital zircon U-Pb ages and the maximum depositional age of modern global sediment: Earth-Science Reviews, v. 203, https://doi.org/10.1016/j.earscirev.2020.103109.

Sharman, G.R., Graham, S.A., Grove, M., and Hourigan, J.K., 2013, A reappraisal of the early slip history of the San Andreas fault, central California, USA: Geology, v. 41, p. 727–730, https://doi.org/10.1130/G34214.1.

Sharman, G.R., Graham, S.A., Grove, M., Kimbrough, D.L., and Wright, J.E., 2015, Detrital zircon provenance of the Late Cretaceous–Eocene California forearc: Influence of Laramide low-angle subduction on sediment dispersal and paleogeography: Geological Society of America Bulletin, v. 127, p. 38–60, https://doi.org/10.1130/B31065.1.

Sharman, G.R., Sharman, J.P., and Sylvester, Z., 2018, detritalPy: A Python-based toolset for visualizing and analysing detrital geo-thermochronologic data: The Depositional Record, v. 4, no. 2, p. 202–215, https://doi.org/10.1002/dep2.45.

Shulaker, D.Z., Grove, M., Hourigan, J.K., Van Buer, N., Sharman, G., Howard, K., Miller, J., and Barth, A.P., 2019, Detrital K-feldspar Pb isotopic evaluation of extraregional sediment transported through an Eocene tectonic breach of southern California's Cretaceous batholith: Earth and Planetary Science Letters, v. 508, p. 4–17, https://doi.org/10.1016/j.epsl.2018.11.040.

Sickmann, Z.T., Paull, C.K., and Graham, S.A., 2016, Detrital–zircon mixing and partitioning in fluvial to deep marine systems, central California, U.S.A: Journal of Sedimentary Research, v. 86, p. 1298–1307, https://doi.org/10.2110/jsr.2016.78.

Simonson, R.R., and Krueger, M.L., 1942, Crocker Flat landslide area, Temblor Range, California: Bulletin of the American Association of Petroleum Geologists, v. 26, no. 10, p. 1608–1631.

Stanley, R.G., 1985, Middle Tertiary Sedimentation and Tectonics of the La Honda Basin, Central California: U.S. Geological Survey Open-File Report 85-596, 263 p., https://doi.org/10.3133/ofr85596.

Stanley, R.G., 1987, New estimates of displacement along the San Andreas fault in central California based on paleobathymetry and paleogeography: Geology, v. 15, p. 171–174, https://doi.org/10.1130/0091-7613(1987)15<171:NEODAT>2.0.CO;2.

Stanley, R.G., 1990, Evolution of the Tertiary La Honda basin, central California, *in* Garrison, R.E., Greene, H.G., Hicks, K.R., Weber, G.E., and Wright, T.L., eds., Geology and Tectonics of the Central California Coast Region, San Francisco to Monterey, Volume and Guidebook: Bakersfield, California, Pacific Section, American Association of Petroleum Geologists, Book GB67, p. 1–29.

Stanley, R.G., and McCaffrey, R., 1983, Extent and offset history of the Ben Lomond fault, Santa Cruz County, California, *in* Andersen, D.W., and Rymer, M.J., eds., Tectonics and Sedimentation along Faults of the San Andreas System: Los Angeles, California, Society of Economic Paleontologists and Mineralogists, Pacific Section, p. 79–90.

Stanley, R.G., Wilson, D.S., and McCrory, P.A., 2000, Locations and Ages of Middle Tertiary Volcanic Centers in Coastal California: U.S. Geological Survey Open-File Report 00-154, 27 p., https://doi.org/10.3133/ofr00154.

Stock, J.M., and Molnar, P., 1988, Uncertainties and implications of the Late Cretaceous and Tertiary position of North America relative to the Farallón, Kula, and Pacific plates: Tectonics, v. 7, p. 1339–1384, https://doi.org/10.1029/TC007i006p01339.

Suppe, J., 1970, Offset of late Mesozoic basement terrains by the San Andreas fault system: Geological Society of America Bulletin, v. 81, p. 3253–3258, https://doi.org/10.1130/0016-7606(1970)81[3253:OOLMBT]2.0.CO;2.

Surpless, K.D., and Beverly, E.M., 2013, Understanding a critical basinal link in Cretaceous Cordilleran paleogeography: Detailed provenance of the Hornbrook Formation, Oregon and California: Geological Society of America Bulletin, v. 125, p. 709–727, https://doi.org/10.1130/B30690.1.

Vermeesch, P., 2013, Multi-sample comparison of detrital age distributions: Chemical Geology, v. 341, p. 140–146, https://doi.org/10.1016/j.chemgeo.2013.01.010.

Wakabayashi, J., 2013, Paleochannels, stream incision, erosion, topographic evolution, and alternative explanations of paleoaltimetry, Sierra Nevada, California: Geosphere, v. 9, no. 2, p. 191–215, https://doi.org/10.1130/GES00814.1.

Wentworth, C.M., Blake, M.C., Jr., Jones, D.L., Walter, A.W., and Zoback, M.D., 1984, Tectonic wedging associated with emplacement of the Franciscan assemblage, California Coast Ranges, *in* Blake, M.C., Jr., ed., Franciscan Geology of Northern California: Society of Economic Paleontologists and Mineralogists, Pacific Section, Book 43, p. 163–173.

Wood, D.J., and Saleeby, J.B., 1997, Late Cretaceous–Paleocene extensional collapse and disaggregation of the southernmost Sierra Nevada Batholith: International Geology Review, v. 39, no. 11, p. 973–1009, https://doi.org/10.1080/00206819709465314.

Zhang, H.-p., Zhang, P.-z., Zheng, D.-W., Zheng, W.-J., Chen, Z.-W., and Wang, W.-T., 2014, Transforming the Miocene Altyn Tagh fault slip into shortening of the northwestern Qilian Shan: Insights from the drainage basin geometry: Terra Nova, v. 26, p. 216–221, https://doi.org/10.1111/ter.12089.

Science Editor: Brad S. Singer
Associate Editor: Michael Smith

Manuscript Received 29 February 2020
Revised Manuscript Received 14 July 2020
Manuscript Accepted 2 September 2020

Printed in the USA